





# Supramolecular structures based on metal-organic cages

# Ehsan Raee<sup>1</sup>, Yuqing Yang<sup>1</sup>, Tianbo Liu\*

School of Polymer Science and Polymer Engineering, The University of Akron, Akron, OH 44325, United States

Keywords: Metal-organic cages, Hierarchical self-assembly, Supramolecular structures, Intermolecular interactions

Molecular metal-organic cages (MOCs) are constructed via coordination among diverse ligands and metal acceptors with great control over the size, shape, cavity, and composition. Their unique and complex molecular structures make different types of intermolecular interactions, including electrostatic, hydrophobic, hydrogen bonding, van der Waals,  $\pi$ - $\pi$  and host-guest interactions *etc.*, possible to coexist in MOC solution. The cooperative or competitive interplay of multiple attractive forces is the driving force leading to exciting and rich solution self-assembly behavior of the MOCs into various supramolecular structures, such as micelles, fibers, nanosheets, nanocubes, nanorods, and blackberry structures. Extensive efforts have been made for gaining better understanding on the formation of these higher ordered structures and designing supramolecular structures with desired properties and functions. In this review, we try to sort out the self-assembly behaviors in MOC solutions from literature based on the type of physical forces involved.

#### 1 Introduction

Metal-ligand coordination-based complexes represent a large group of highly diverse compounds. The directional metal-ligand coordination bonds make it possible to predict and control the final structures of the products, regardless of its complexity [1]. Metal-ligand coordination bonding can achieve the syntheses of defect-free products under ambient conditions when compared with classic synthesis strategies involving covalent bonding formation [2,3]. Pioneering works by Fujita [4,5], Stang [6,7], Newkome [8], Nitschke [9,10], etc. laid the foundation for building up metal-organic complexes, developed novel coordination-based compounds with diverse shapes and geometries such as 2D metal-organic macrocycles (MOMs) including triangles [11],

Supramolecular chemistry is to design and build diverse functional structures with tunable properties [31–43] via various noncovalent interactions [44] including hydrogen bonding

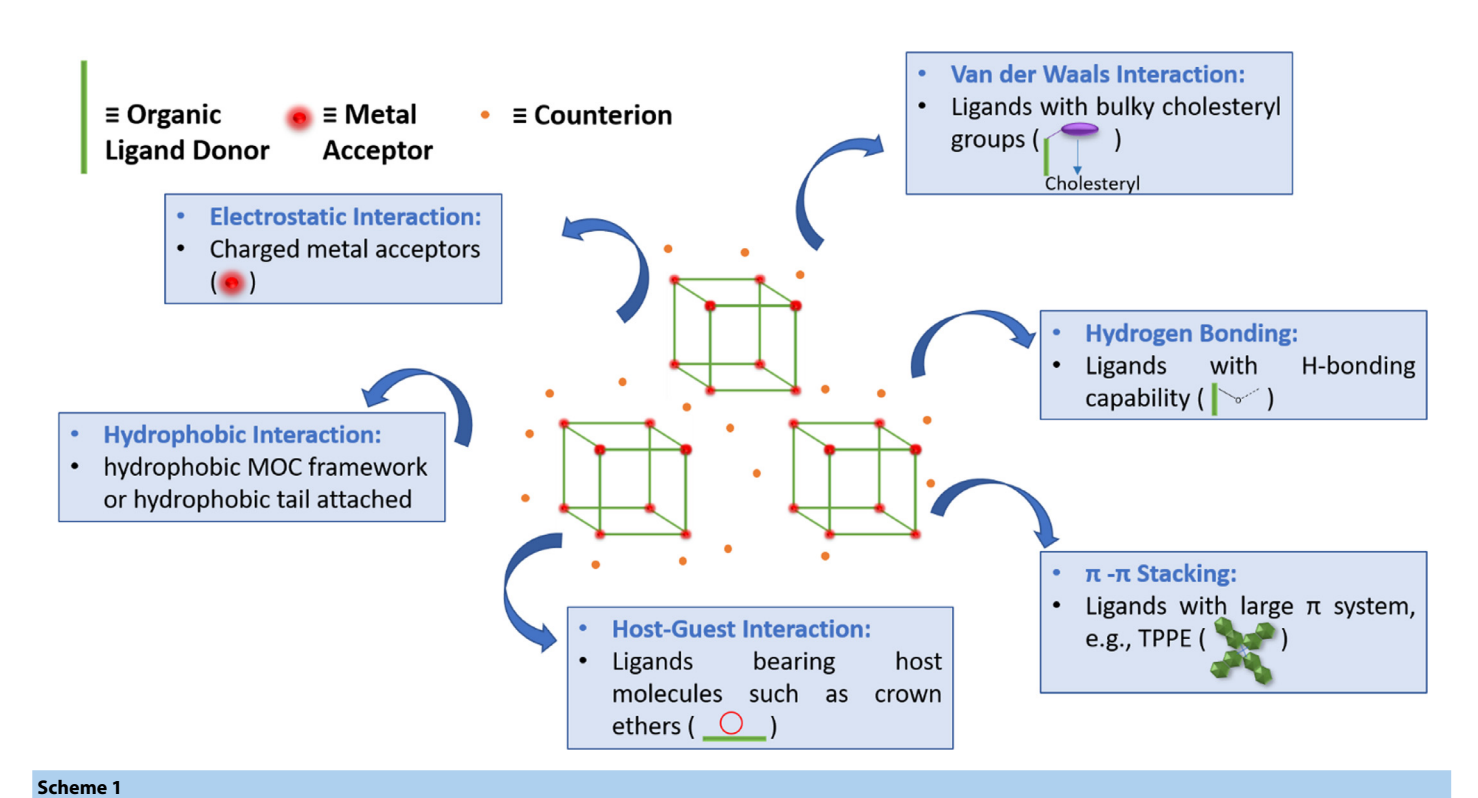
Received 17 December 2020; Received in revised form 20 January 2021; Accepted 20 January 2021

rectangles [12], squares [13], rhomboids [14,15], and 3D metalorganic cages (MOCs) including tetrahedron [16], cube [17], octahedron [18], cuboctahedron [19], trigonal prism [20,21], tetragonal prism [22], hexagonal prism [23], etc. Among these complexes, MOCs have gained more attention due to their variety of shapes and controllable pore sizes. These features make MOCs better options for host-guest chemistry, and promising materials with tunable functionalities for catalysis [24,25], drug delivery [26,27], sensing [28,29], and others [30]. Currently, extensive work has been focused on the construction of MOCs, achieving tunable molecular pore sizes and diverse functions, whereas the weak non-covalent intermolecular interactions among MOCs and the consequent supramolecular structures have been rarely summarized systematically, although related studies have been reported frequently in literature.

<sup>\*</sup> Corresponding author.

E-mail address: tliu@uakron.edu (T. Liu).

Both the authors contributed equally to this work.



Schematic representation of MOCs' structure, and how presence of metal ions or functional ligands in their structure can generate different physical intermolecular interactions between MOCs.

[45,46], van der Waals [47,48],  $\pi$ - $\pi$  stacking [49,50], solvophobic [51,52], and electrostatic interactions [53–55] between the building blocks including MOCs. Almost all MOCs are made up of transition metals and organic ligands. These two components could generate multiple types of basic intermolecular interactions (Scheme 1), leading to not only very sophisticated conditions in solution, but also rich self-assembly behaviors and supramolecular structures. The charged metal ions can induce electrostatic interaction, in many cases involving counterion-metal ion interaction and solvation; [56] they could also interact with each other such as Pt...Pt in Pt-based MOCs [57], or form coordination bonds with other species in solution. The organic ligands can be easily tuned during their synthesis with different functional groups [9,58-61] to generate intermolecular interactions such as hydrophobic, hydrogen bonding,  $\pi$ - $\pi$ interactions, etc. The simultaneous presence of multiple physical forces sometimes makes it difficult to understand MOC solutions; but it also provides extensive opportunities for adjusting the relative strengths of these interactions among MOCs with rational molecular design or changing external conditions (e.g., temperature or solvent polarity), leading to the formation of diverse supramolecular structures.

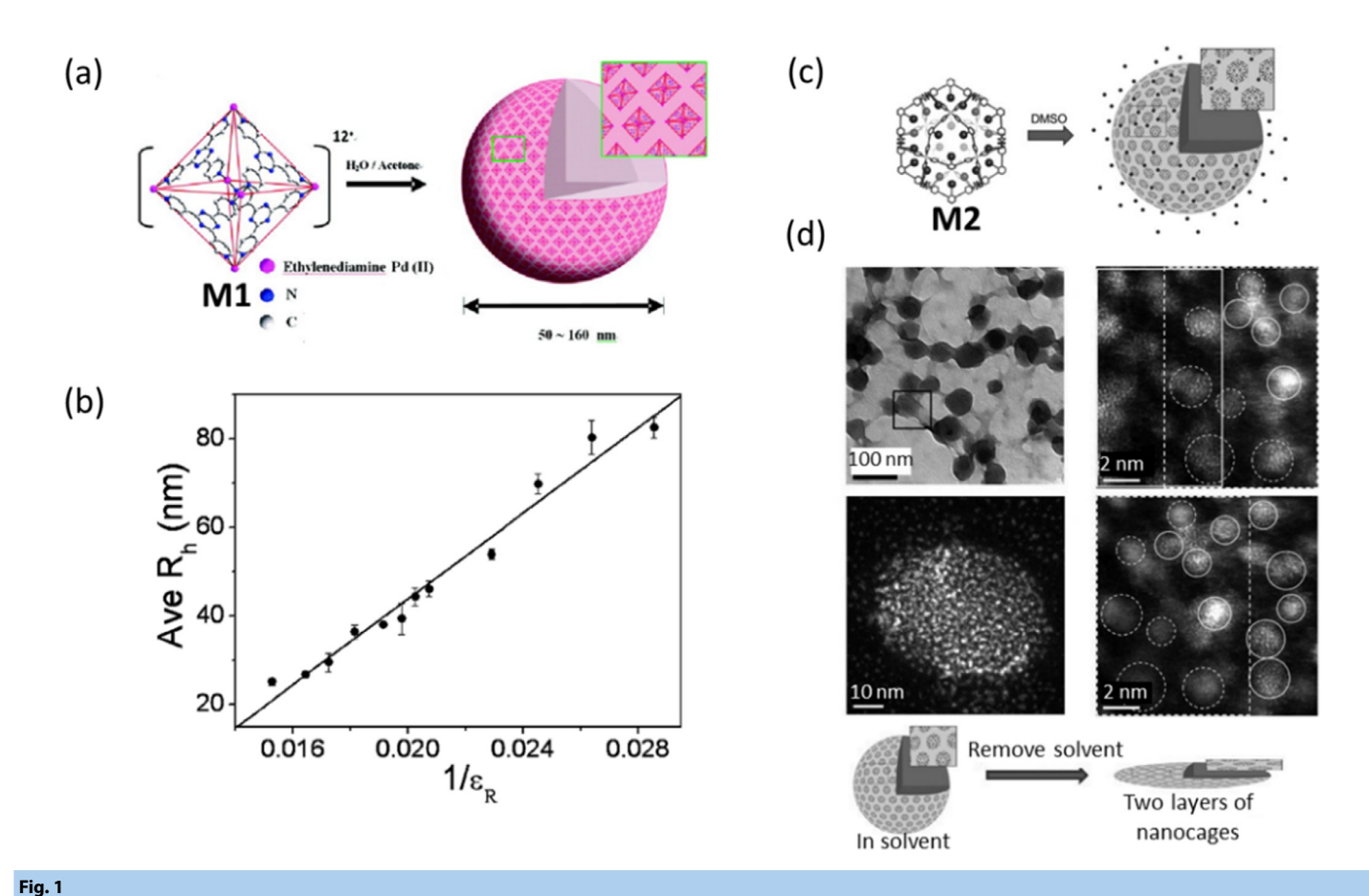
Here, we review the physical interactions among MOCs that lead to supramolecular structure formation. The article is categorized based on the major attractive physical forces which regulate the assembly process. In Scheme 1, it is represented that how the presence of different components in the structure of MOCs can induce various intermolecular interactions between them. Also, unique functions and properties of MOC-based supramolecular structures are discussed as well. We did not

include the work in which assembly structures were formed by a secondary coordination bonding between cages [62], as it is usually considered a chemical rather than a physical interaction.

#### 2 Electrostatic interaction between MOCs

Electrostatic interaction between charged MOCs can often be dominant if the MOCs are in polar solvents and have small, less polarizable counterions, both leading to higher net charge on the MOCs. Less bulky or more hydrophilic organic ligands would further strengthen the role of electrostatic interaction. The charge-dominated MOCs show high solubility in polar solvents and typical macroionic solution behavior. Macroions cannot be described by either Debye-Huckel theory [63] for small ions or DLVO theory [64] for colloids - significant but not dominant counterion association around single soluble MOCs occurs in solution. Macroions show different binding mechanism and strength to different counterions [65-67], and the consequent counterion-mediated attraction can induce selfassembly behaviors, in many cases into single-layered hollow spherical blackberry-type structures [43,68]. Inter-macroionic distance in blackberry structures (and consequently reflected on the blackberry structure size) can be slightly tuned by adjusting the charge density of macroions using solvent polarity, counterions type, or solution ionic strength [55,69].

The self-assembly of MOCs into blackberry structures was first reported by our group [56,70]. An octahedron  $Pd_6L_4$  MOC (Pd=ethylenediamine palladium, and L=2,4,6-tris(4-pyridyl)-triazine) (**M1**) with 12 positive charges self-assembles into blackberry structures in water/acetone mixed solvent (Fig. 1a). The linear relationship between size of the assemblies and the



(a) Schematic representation of the structure of  $\mathbf{M1}$  and its self-assembly process into blackberry structure. (b)  $R_h$  of blackberry structures assembled at different ratios of acetone/water versus inverse dielectric constant of the mixed solvent. (c) Schematic representation of the self-assembly process of  $\mathbf{M2}$  into blackberry structures and distribution of nitrates (small dots). (d) TEM and SEM images of blackberry structures assembled by  $\mathbf{M2}$ , revealing that some of them are collapsed due to solvent evaporation. Adapted with permission from refs 56 and 70. Copyright © 2008, American Chemical Society and 2011 Wiley-VCH.

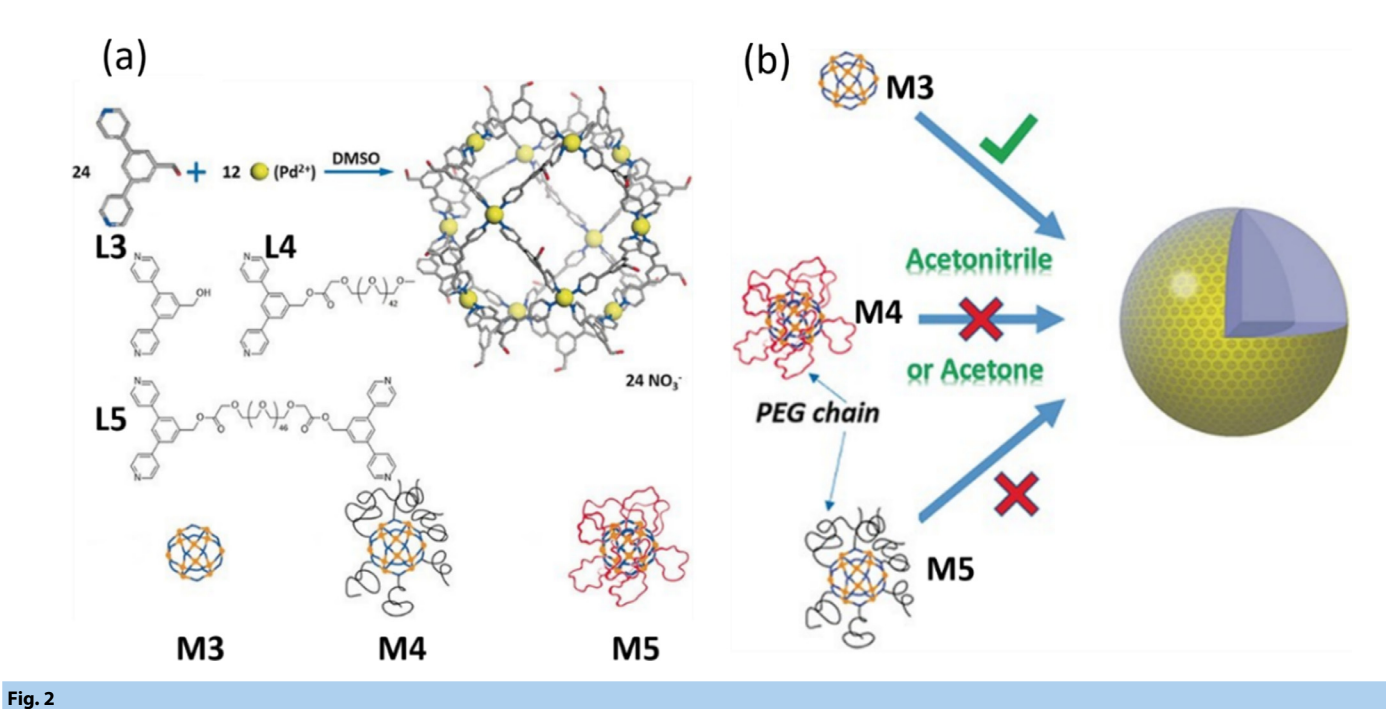
inverse dielectric constant of the solvent (Fig. 1b) indicates that the counterion-mediated attraction is the major driving force of the self-assembly process [71]. Then, we reported the self-assembly of another MOC, cuboctahedron Fujita type  $M_{12}L_{24}$  (M=Pd and L=2,6-bis(4-pyridylethynyl)toluene) (**M2**), into single-layered blackberry structures in DMSO by the addition of extra nitrates as counterions (Figs. 1c) with more direct evidence on the single layer nature of the assemblies. It was shown that increasing ionic strength of the solution results in size increment of the blackberry structures. The single layer feature of the blackberry structures was further confirmed by SEM studies (Fig. 1d). Besides, calculations based on Zimm plot indicated that 956±81 of MOCs are distributed on the surface.

The self-assembly of MOCs into blackberry structures follows the same mechanism of other macroions, that is, the counterion-mediated attraction between MOCs. However, MOCs can be better model macromolecules to mimic biological processes such as viral capsid formation due to their more complex structure which can introduce several types of intermolecular interactions to the supramolecular assembly process, like what we observe in biological systems.

If keeping MOCs as single macroions in solution is desired, one way is to use bulkier organic ligands to prevent the MOCs moving

close to each other. For example, for non-PEGylated  $Pd_{12}L_{24}$  MOC (L=(3,5-di(pyridine-4-yl)phenyl)-methanol) (M3), and two PEGylated ones (M4 and M5), with ligands being on the periphery of the cage (Fig. 2a) [72], M3 self-assembles into blackberry structures in acetone and acetonitrile; while M4 and M5 tend to remain as discreet macroions under the same conditions (Fig. 2b). The bulky ligands of PEGylated cages decrease the non-specific interactions between M4 (or M5) and their counterions, inhibiting them coming close to each other and self-assembling into blackberry structures. This work indicates that tuning the functionality of MOCs can control the assembly/disassembly of the MOCs in the solution, which is beneficial to their applications.

One important question related to the homochirality phenomenon is that how chirality affects the intermolecular interactions leading to the assembly of homochiral supramolecular structures. MOCs bearing chiral moieties can be used as an ideal model to mimic naturally occurring homochiral assembly processes. For that, chirality was induced to the charged  $Pd_{12}L_{24}$  by functionalizing it with D- or L-alanine on the periphery (**M6**) (Fig. 3a) [73]. The chiral cages can self-assemble into blackberry structures with extra nitrates as original counterions. With some additional small chiral counterions (e.g.,



(a) Structure of the non-PEGylate (M3) and PEGylated (M4 and M5) cuboctahedra MOCs and their ligands (L3, L4, and L5). (b) M3 can self-assemble into blackberry structures in acetone and acetonitrile; while, PEGylated cages M4 and M5 remain as discreet macroions. Adapted with permission from ref 72. Copyright © 2016 Wiley-VCH.

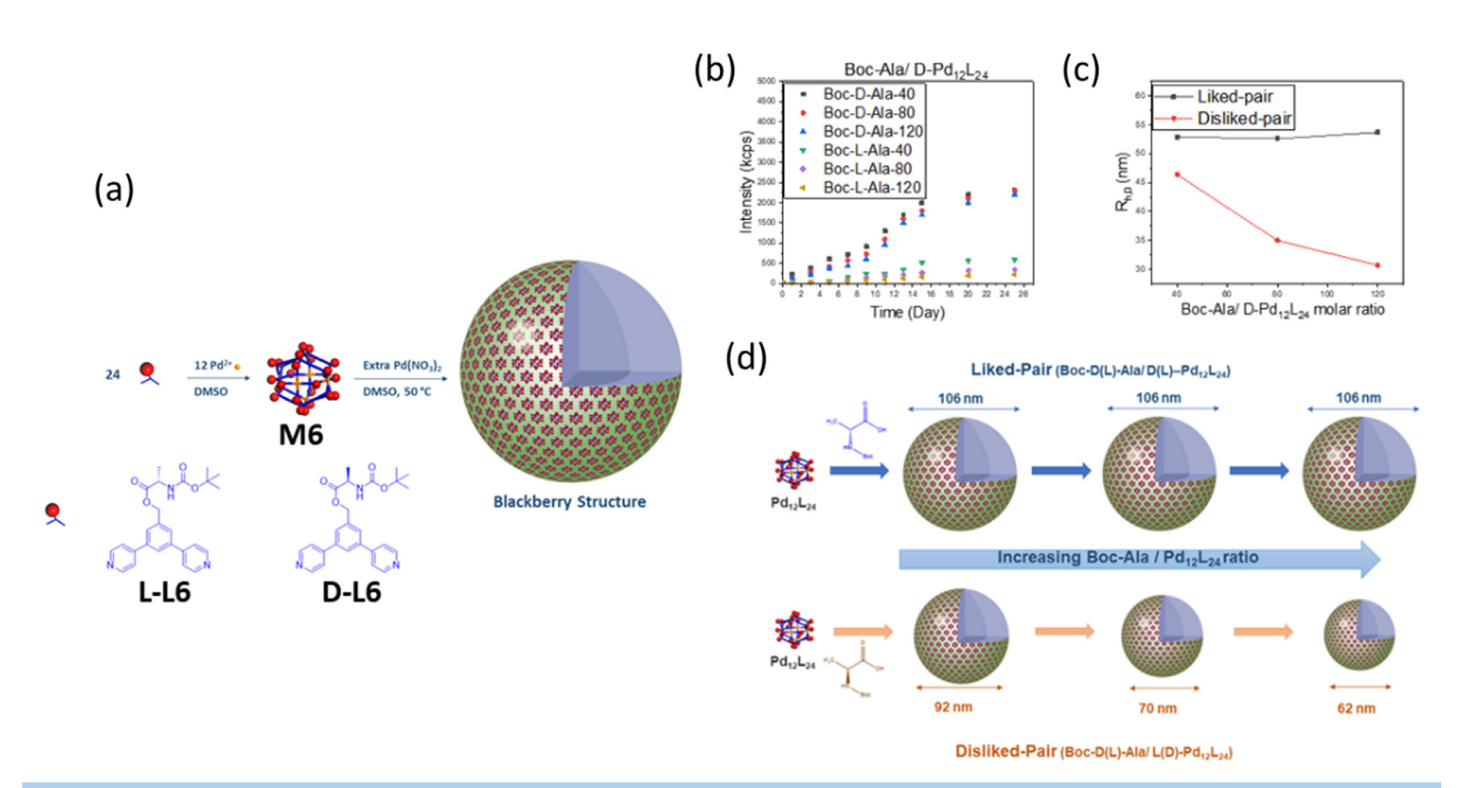
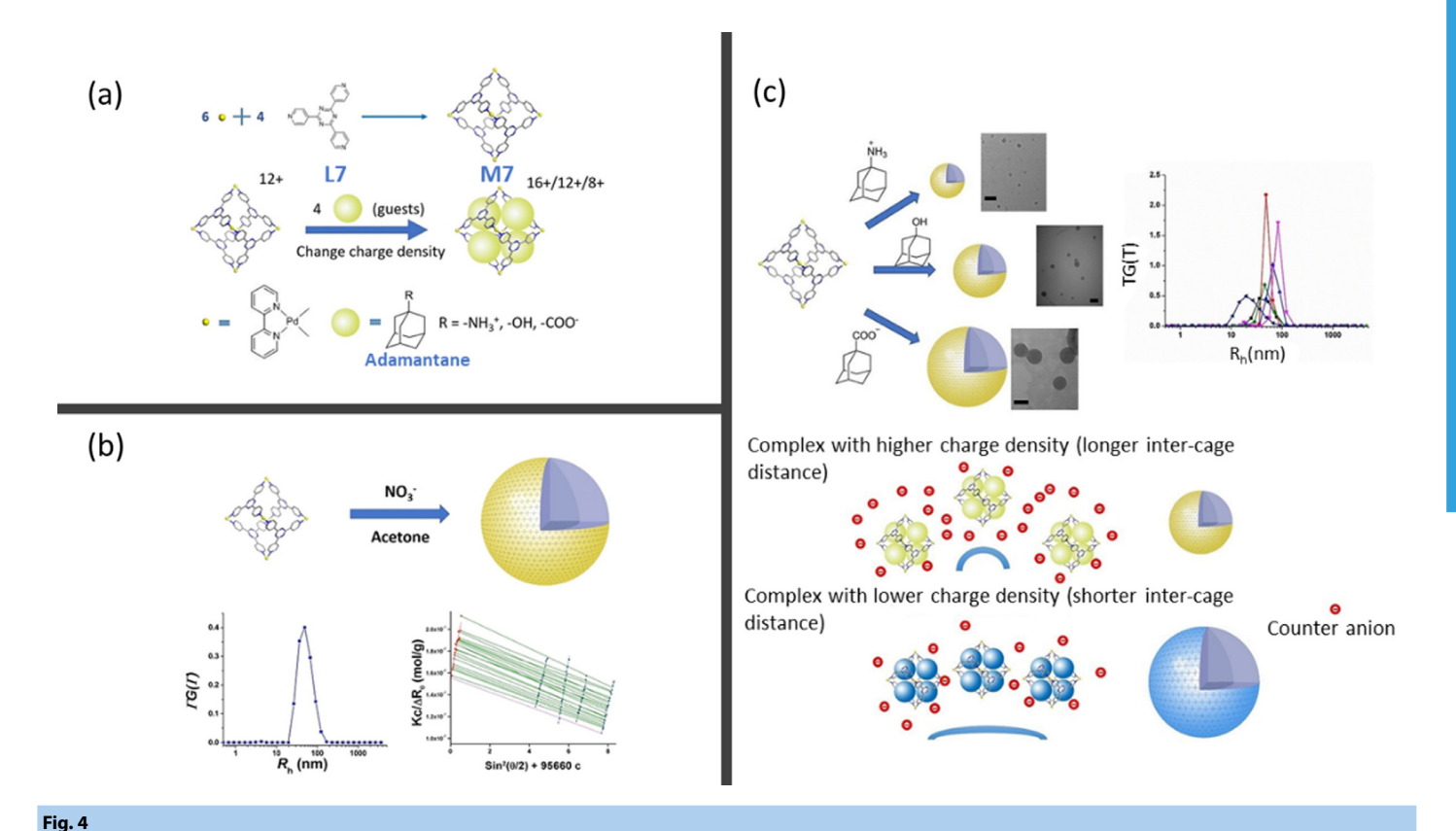


Fig. 3

(a) Schematic representation of **M6** and its chiral ligands **D-** and **L-L6**, and the self-assembly of **M6** into blackberry structures. (b) SLS scattered intensity of **M6** self-assembly process versus time at the presence of different amounts of Boc-D and L-alanine. The lower scattered intensity of the disliked-pairs indicates self-assembly suppression in these pairs. (c) Size of the blackberry structures versus Boc-alanine/ **M6** ratio. Blackberry size decreases for disliked-pairs as this ratio increases; while, for liked-pair, blackberry size remains almost constant. (d) Schematic representation of Fig. 3c. Adapted with permission from ref 73. Copyright © 2020, American Chemical Society.



(a) Structure of octahedron MOC  $\mathbf{M7}$  and its ligand, and schematic representation of encapsulating adamantane guests. (b) Self-assembly of  $\mathbf{M7}$  into blackberry structures in acetone (top), and  $R_h$  distribution and Zimm plot of the assemblies (bottom). (c) Schematic representation of the effect of guest molecules on the size of the blackberry structures (top). Positively charged guests increase surface charge density of  $\mathbf{M7}$  and inter-cage distance (middle). Negatively charged guests decreases surface charge density and inter-cage distance (bottom). Adapted with permission from ref 74. Copyright © 2019 Wiley-VCH.

Boc-alanine) in the **M6** solutions, the D-cages and L-counterions (disliked-pairs in Fig. 3) interact more strongly than the D-cages and D-counterions (liked-pairs), partially inhibiting the nitrate-cage binding, leading to a partial suppression of the self-assembly, and smaller size of the blackberry assemblies than the liked-pairs. Same behavior was observed for the L-cages and D-counterions. This study provided some additional evidence on the mechanism of the homochirality phenomenon, particularly for the evolution from macromolecular to supramolecular level via electrostatic interaction.

The charge density of MOCs can be controlled by encapsulating charged molecules inside MOCs. An octahedron  $M_6L_4$  ( $M=Pd^{II}(2,2'-bipyridine)$ , L=2,4,6-tri(4-pyridyl)-1,3,5-triazine) MOC (M7) can encapsulate up to four (positively/negatively) charged or neutral adamantane (Fig. 4a) [74]. M7 self-assembles into blackberry structures with an R<sub>h</sub> of ~42 nm and molecular weight of  $6.4\times10^6\ \text{g/mol}$  in acetone when there are no guest molecules within its cavity (Fig. 4b). While encapsulating neutral guests did not alter the assembly size, charged adamantanes could significantly change it. Negatively charged guests decreased the charge on M7 from 12 to 8, and the lower surface charge of the complex led to shorter inter-cage distance, and thus larger blackberry structures ( $R_h = 67$  nm). Moreover, the charge of M7 complex could be increased to 16 by encapsulation of four positively charged guests which resulted in smaller blackberry structure with  $R_h=21\ nm$  (Fig. 4c). This study involves host-guest feature of MOCs as another method to tune the charge of MOCs and the strength of their intermolecular electrostatic interaction.

Although being responsible for the assembly size change, the small change of the inter-MOC distance in the blackberry assemblies is difficult to accurately measure directly. Interestingly, it can be revealed by incorporating fluorescent-active ligands in the MOCs. With tetra(4-pyridylphenyl)ethylene (TPPE), a common aggregation-induced emission (AIE) chromophore, being incorporated into MOCs [75]. The blackberry structures of M8 in ethyl acetate show cyan emission (Fig. 5) [76]. At higher M8 concentrations their charge density becomes lower, leading to stronger electrostatic attraction between M8 in the blackberry structures, making them closer and forming larger assemblies. The inter-M8 distance in blackberry structures is longer than it in aggregates/precipitates (traditional AIE situation), therefore the emission wavelength from the solution of M8 blackberry structures (503 nm) is longer than its AIE wavelength (454-477 nm), and increases monotonically (from 503 to 511 nm) with smaller blackberry structures (Rh from 90 to 40 nm), i.e., longer inter-cage distance, suggesting a decrease of degree of conjugation in TPPE. Therefore, functionalizing MOCs with luminescence groups might help us to detect any tiny change in the intermolecular electrostatic interaction by correlating the wavelength change to the change of intermolecular distance in the assemblies.

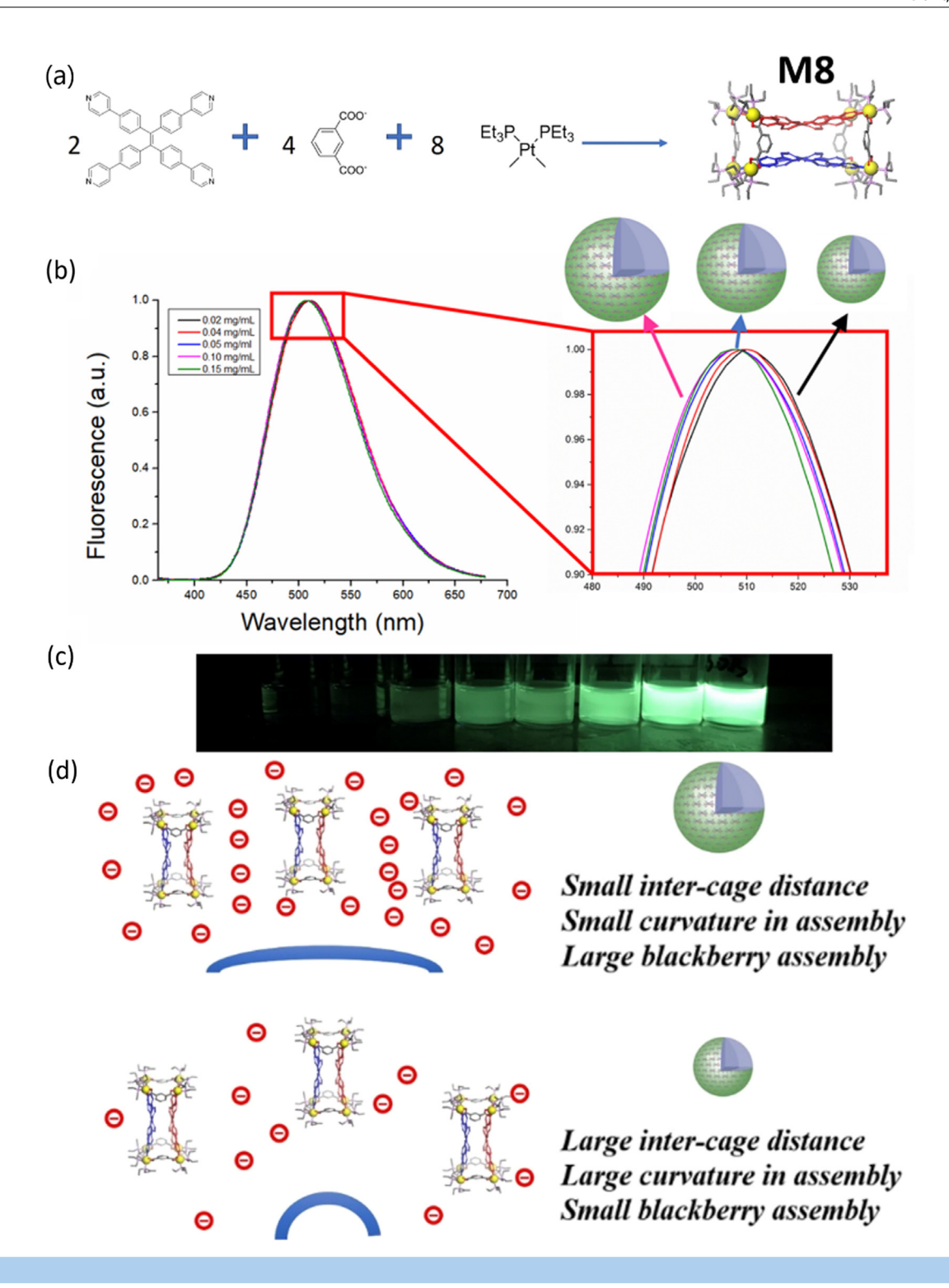


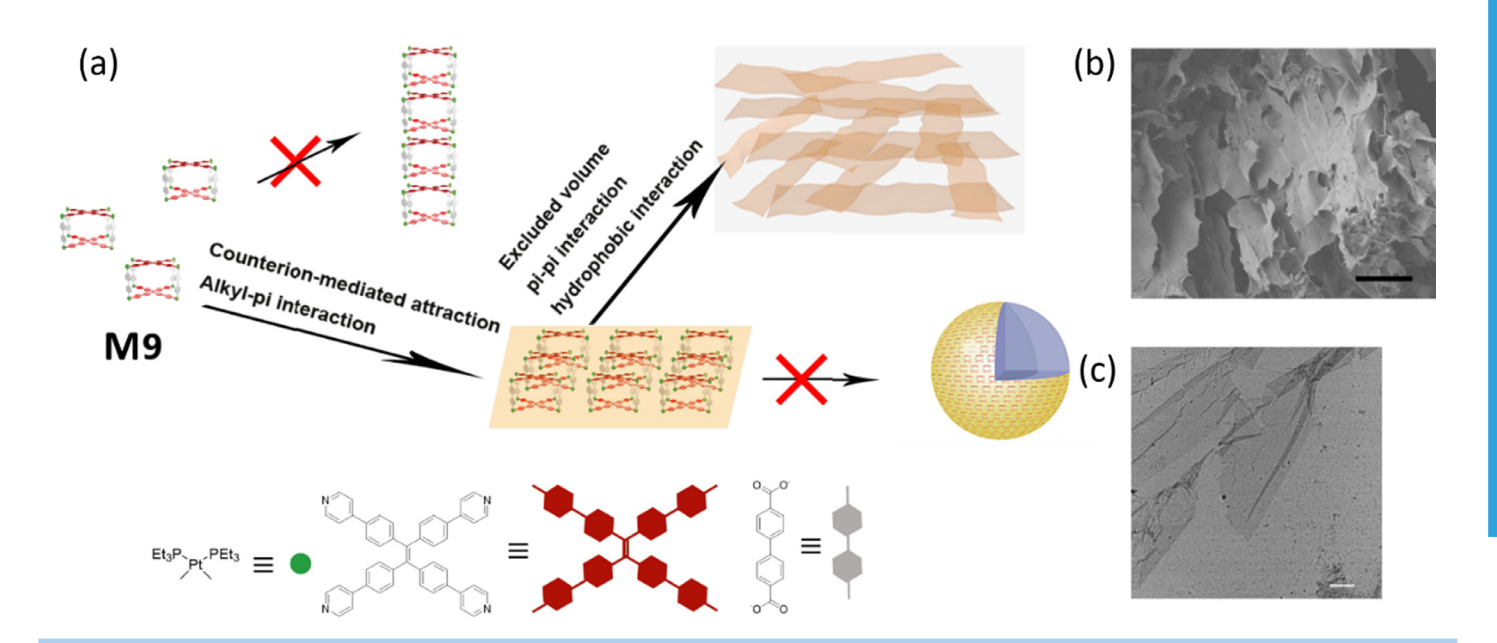
Fig. 5

(a) Molecular structure of **M8**. Red and blue: tetrakis(4-pyridylphenyl)ethylene, TPPE; gray: isophthalate and triphenylphosphine; yellow: platinum(II). (b, c) Fluorescence spectra and photograph of concentration dependence of **M8** assembly fluorescence (normalized) in ethyl acetate excited at 355 nm. (d) The relationship between intercage distance, curvature in the assembly, assembly size in the blackberry structure, and fluorescence. Adapted with permission from ref 76. Copyright 2019 American Chemical Society.

Another study on the self-assembly of MOCs into blackberry structures was conducted by Wang et al. A terpyridine-based hexapodal ligand ( $\mathbf{L}$ ) was synthesized to obtain a  $Zn_{12}L_4$  MOC with 24 positive charges, and the self-assembly process was studied in MeOH/CH<sub>3</sub>CN mixed solvent [77]. All

the studies discussed so far indicate that various types of MOCs with different size, geometry, and functions can self-assemble into blackberry structures if intermolecular electrostatic interactions are controlled by tuning the surface charge of the MOCs.

Fig. 6



(a) Schematic showing the self-assembly of **M9** into nanosheet, leading to hydrogel. (b) SEM images of freeze-dried hydrogel from **M9**. Scale bar: 100  $\mu$ m. (c) TEM images of 5 mg/mL **M9** solution with 8 equivalents of NaNO<sub>3</sub> with scale bar: 1  $\mu$ m. Adapt permission from ref 78. Copyright © 2020, American Chemical Society.

Blackberry structure formation requires the bending and closing of the 2-D sheets assembled by the MOCs. If the inter-MOC distance continues to decrease due to stronger attraction, bending will become very difficult and eventually the 2-D sheets will remain in solution. Their large excluded volume might generate gelation. When isophthalates in M8 were replaced by biphenyl dicarboxylates (M9) [78], it maintains a more rigid conformation than that of M8 in water. M9 self-assembles into 2D nanosheets with the addition of salts. These stiff nanosheets are difficult to bend into 3D hollow spherical blackberry structures. Instead, they remain as 2D sheets in solution. The nanosheets further stack, facilitated by hydrophobic and  $\pi$ - $\pi$  interactions, to construct a MOC hydrogel (Fig. 6). The gels might return to solution state when replacing the salts, indicating the counterion-mediated attraction is essential for the gelation. Other MOC-based gelation processes have been discussed later, mainly involving van der Waals, host-guest and  $\pi$ - $\pi$  interactions *etc*.

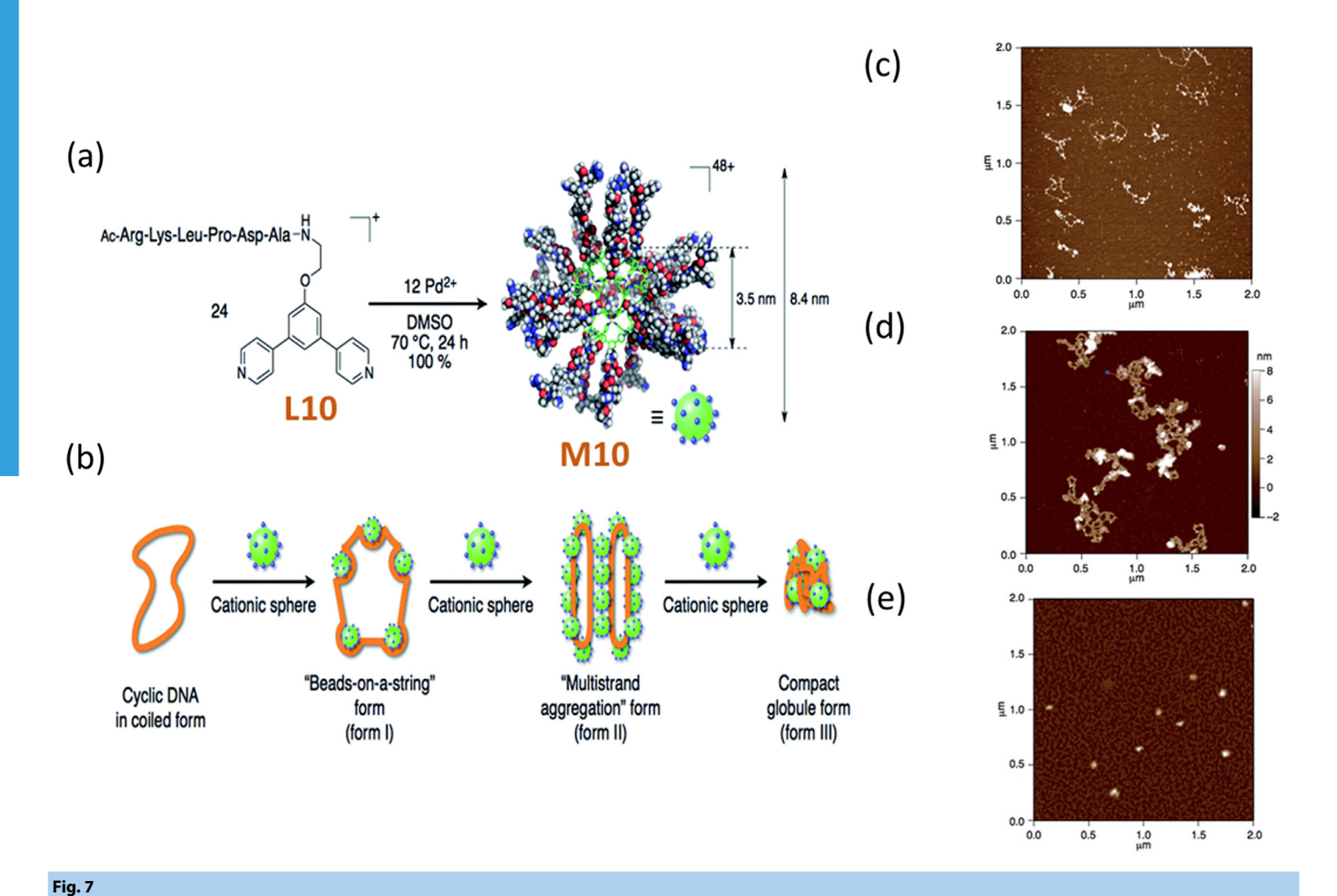
Mimicking naturally occurring self-assembly processes is one of the most interesting aspects of studying the inter-MOC interactions. A positively charged cuboctahedron MOC covered with peptide chains (M10) was reported to mimic DNA condensation process through a three-step self-assembly process at the presence of a negatively charged coiled DNA [79]. M10 was used as a model system due to its similar size and charge density to histone octamer. Depending on the total charge ratio of M10/DNA(=Z), three types of structure were assembled: first, when Z = 0.87 a "beads-on-a-string" structure was observed by AFM (Fig. 7c), then Z was increased to 1.7 and multistranded structures were detected (Fig. 7d), and finally, a compact globular form was assembled when Z was further increased to 8.7 (Fig. 7e). This study is another example of great capability of MOCs to model naturally occurring assembly systems due to their tunable charge, size, structure, and function.

# 3 Hydrophobic interaction between MOCs

Hydrophobic interaction is dominant for MOCs possessing bulky, hydrophobic organic domains; and it becomes more prominent in polar solvents. For most MOCs, their multiple hydrophobic domains are separated by corner metal ions, i.e., there exist multiple small hydrophobic domains rather than one or a few major ones, such as amphiphilic block copolymers or surfactants. In such a case, the hydrophobic domains often affect the solubility of MOCs in solution. After further modifications, the hydrophobic domains could become more dominant, and lead to versatile assembly behaviors similar to surfactants. However, the unique molecular architecture, size, and structural stiffness of MOCs make their self-assembly behavior more complicated.

Amphiphiles with a giant polar part and single or multiple carbon tails can be constructed by using MOCs. Reversibly, amphiphiles with hydrophobic core (or head) and hydrophilic tails can be constructed as well. M11 is made by mixing tetraphenylethene (TPE)-based sodium benzoate ligands with organicplatinum(II) acceptors and PEG-modified dipyridyl ligands as pillars (Fig. 8) [80]. Although the inner framework of M11 is hydrophobic, it has good solubility in water due to the attached PEG chains. Nanospheres with an average diameter of 140 nm were formed by M11 based on hydrophobic interaction. In the proposed model for the nanospheres, hydrophobic framework of the MOCs were in close contact at the core of the nanospheres and hydrophilic PEG chains were in contact with water bending radially outward the nanospheres. It is obvious that endowing amphiphilic features to the MOCs can lead to the assembly of structures different from what was obtained by highly charged MOCs due to electrostatic interaction between them.

The same idea was used to synthesize two amphiphilic MOCs with hydrophobic cuboid framework and PEG-based

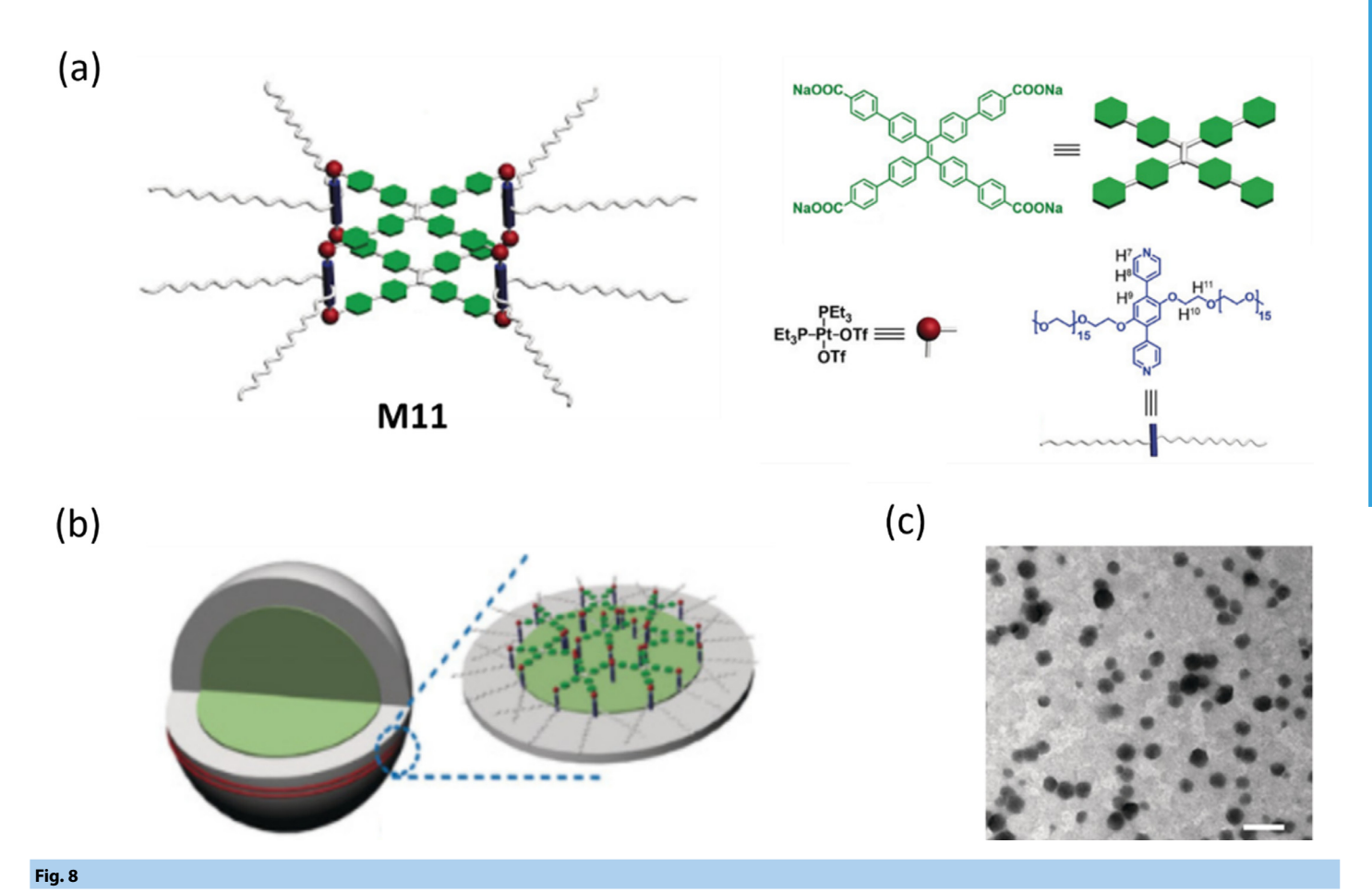


(a) Peptide covered **M10** and its ligand (**L10**) structure. (b) Schematic representation of stepwise assembly process of **M10** and a cyclic coiled form DNA (pBR322 DNA). (c), (d) and (e) AFM images of beads-on-a-string, multistrand, and globular assemblies, respectively. Adapted with permission from ref 79. Copyright © 2014, Royal Society of Chemistry.

hydrophilic tails which keep different amount of hydrophilic tails: one has four hydrophilic tails [81] and the other one has twelve [82]. The amphiphilic nature allows them to assemble into various supramolecular structures in water. When MOCs carry bulkier hydrophilic tails, they tend to form vesicles instead of nanospheres at low concentrations. With increasing concentration, both assemblies transformed into nanofibers, which are not thermodynamically stable and further formed nano-ribbons, if MOCs are attached with less hydrophilic tails. The hydrophobic core arranged themselves orderly based on  $\pi$ - $\pi$  interactions, and the PEG chains extend radially from the framework. These two studies reveal that by tuning the length and number (or volume) of the hydrophilic chains in the structure of amphiphilic MOCs, intermolecular hydrophobic interaction can be controlled, resulting in various supramolecular structures.

An amphiphilic tetragonal MOC M12 [83] was made by one hydrophilic head and two hydrophobic tails. M12 contains square-planar metal acceptors, together with two shapematching pairs of different bis-monodentate ligands, dodecylfunctionalized acridone-based ligands, and methoxy-modified phenanthrene-derived ligands (Fig. 9). The nonpolar dodecyl-modified ligands and the hydrophilic methoxy-functionalized ligands with charged Pd ions endow the amphiphilic nature to **M12**. Polydispersed vesicles were observed in acetonitrile and acetonitrile-water mixture with diameters in a broad range of 200–1000 nm and 100–1500 nm, respectively, whereas in DMSO/water mixed solvent, the monodispersed vesicles were formed with diameters ~200 nm. Solvent polarity could be the key on determining the strength of inter-MOC hydrophobic interaction leading to polydispersed or monodispersed supramolecular structures.

Similar to surfactants, the length of the hydrocarbon tail plays a critical role in the strength of hydrophobic interaction between amphiphilic MOCs. Interlocked M<sub>8</sub>L<sub>16</sub> MOC (**M13**) was synthesized by two different routes (Fig. 10a and 10b) [84]. From **M¹13** to **M³13**, the length of the carbon tail in the ligand's structure increases, endowing more hydrophobicity to **M13**. **M¹13** and **M²13** remained as discrete MOCs in acetonitrile solution, but **M³13** with the longest hydrocarbon tail self-assembled into vesicular structures. Moreover, the self-assembly process was thermoreversible. Vesicles were disassembled at



Molecular structure of **M11**. Green: TPE-based sodium benzoate ligands; Red: Organicplatinum(II) metal acceptor; Blue: PEG-modified dipyridyl ligand. (b) Schematic showing self-assembly of **M11** into nanospheres. (c) TEM image of nanospheres formed by **M11** in water. Adapted with permission from ref 80. Copyright © 2019 Wiley-VCH.

elevated temperatures (50–70 °C) and again assembled when temperature is cooled down to 20 °C (Fig. 10e).

All the studies mentioned in this section indicate that several factors can affect the hydrophobic interaction between MOCs, including the structure of the amphiphilic MOC (i.e., having hydrophilic framework and hydrophobic tail or vice versa.), length and number of the tails, and solvent quality. Tuning these parameters can achieve building up different supramolecular structures with different potential functions and features.

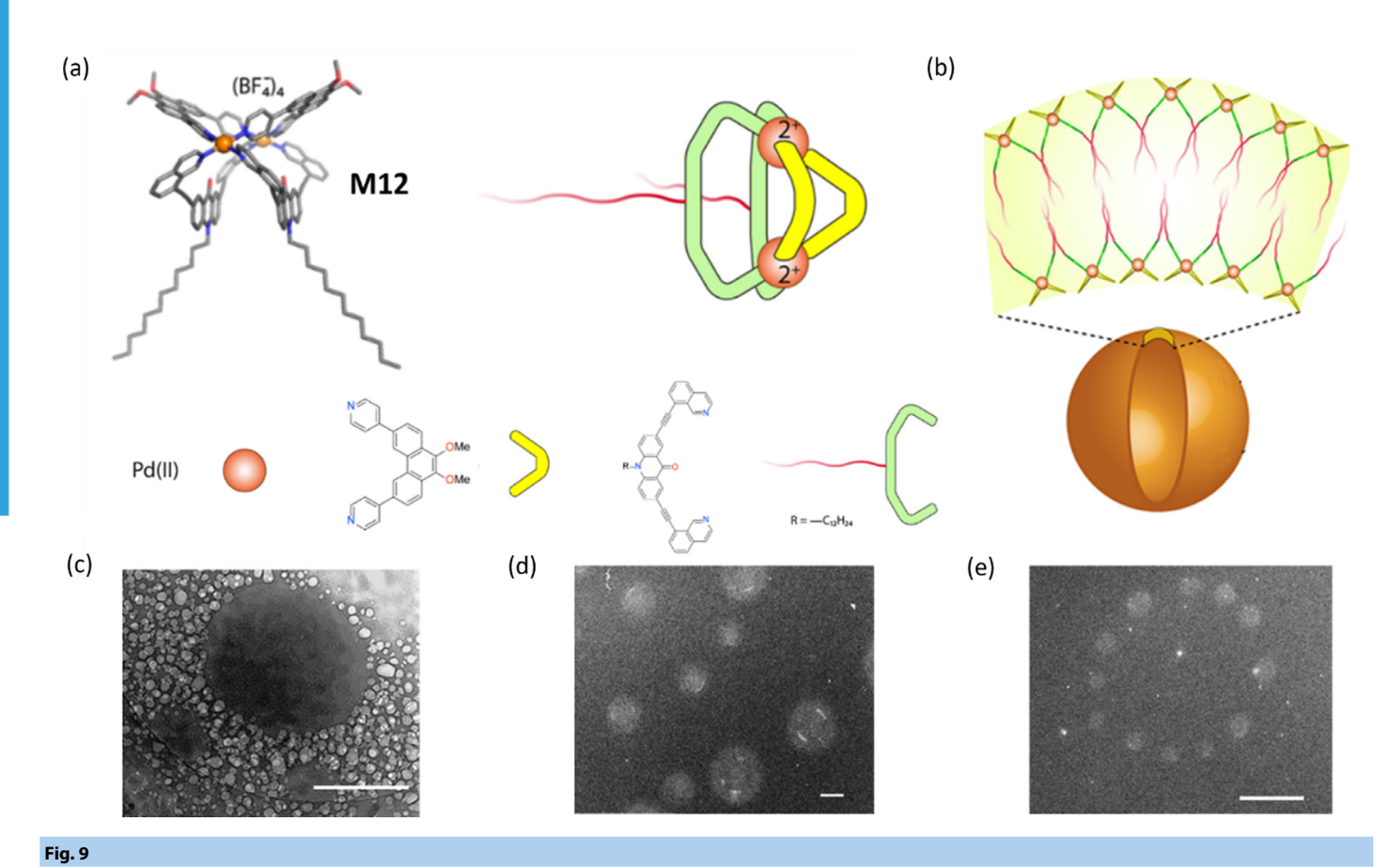
# 4 Host-guest interaction between MOCs

The empty spaces inside MOCs and the functional groups on the sides of MOCs provide multiple sites for accommodating or binding proper small species, leading to the unique host-guest interaction. This key feature results in very diverse applications of MOCs. Here are some examples to show how the host-guest chemistry can affect the assembly of MOCs in solution.

Crown ethers are a type of macrocyclic polyether which contains multiple oxygen methylene units, commonly used as host to cations and neutral molecules due to its strong binding affinity [85]. Taking this advantages, 21-crown-7 (21C7) moieties

were introduced in the pillar parts, coordinated with TPE-based sodium benzoate ligands and organicplatinum(II) acceptors to obtain M17 [86]. With the addition of bis-ammonium linkers, a self-healing and stimuli-responsive supramolecular gels with interconnected porous structures was formed via host-guest interactions. The gel shows thermally induced and potassium-ion-induced gel-sol transitions, since both weaken the host-guest interaction between 21C7 and bis-ammonium linkers, and therefore the gel can be recovered by cooling or further adding 18-crown-6. The stiff gel from M17 indicates a simple and highly efficient strategy for constructing stimuli-responsive and self-healing robust supramolecular material, showing promise for the MOCs into smart soft materials.

In another example of using crown-ether-decorated ligands to trigger host-guest interaction in MOC system [87], the tetragonal MOC **M18** was obtained via coordination between metal acceptors Zn(II) and the elaborate metal-organic ligands, which contain one benzo-21-crown-7 (B21C7) functionalized terpyridine and three 120-degree-bent bis terpyridines linked via the terpyridine-Ru<sup>2+</sup>-terpyridine coordination bonds. The host-guest interaction between B21C7 in cages and alkyl-ammonium salt was observed when **M18** and bis-ammonium salt were mixed



(a) Molecular structure of M12. (b) Cartoon representation of vesicles self-assembled from M12 in the presence of polar solvents or solvent mixtures (acetonitrile, acetonitrile—water, and DMSO—water). (c) Cryo-TEM images of M12-based vesicles formed in acetonitrile. Scale bar: 500 nm. HAADF-STEM image of vesicles obtained by M12 in (d) acetonitrile-water mixture and (e) DMSO-water mixture with scale bar: 500 nm. Adapted with permission from ref 83. Further permissions related to the material excerpted should be directed to the ACS. Copyright © 2018 American Chemical Society, https://pubs.acs.org/doi/abs/10.1021/jacs.8b10991.

in acetonitrile/water mixed solution, leading to supramolecular networks and gelation. Within the system, several structures were observed, such as intertwined dimers, oligomers, and the dominant host-guest-based supramolecular polymer, which is indicated by the entangled, extended, and interconnected fibrous network as shown in Fig. 12.

Pillar[n]arenes are widely used as a new type of macrocyclic host compared to crown ethers, not only due to their pillar-shape structures and ease of functionalization but also the extensive host-guest recognition capabilities especially for neutral guests. Since their discovery in 2008, pillar[n]arenes have been a popular family of macrocyclic arene hosts due to their accessible one-step synthesis, convenient functionalization, symmetrical prism structures and perfect cavity host-guest properties. Compared with other macrocyclic hosts, the most peculiar recognition behavior of pillararenes is the strong binding affinity of pillar [5] arenes (P5As) towards neutral guests in organic media, which is unfeasible for classic crown ethers and calixarenes [88].

With pillar [5] arene linked to pyridyl ligands, together with square-planar Palladium(II) acceptors, **M19** was prepared (Fig. 13) [89]. **M19** maintains a tetragonal conformation with four pendent pillar [5] arene, which work as macrocyclic hosts.

With the addition of neutral ditopic guest molecules into a chloroform solution of M19, 3D interconnected porous structures and gelation were observed, which were caused by host-guest interaction between the extra ditopic guest molecules and pillar [5] arene of M19. Based on the dynamic nature of the host-guest interaction, the supramolecular gel shows temperature and pH response. Moreover, the MOC's cavity was used for controlled drug release. Emodin, as drug molecules, were encapsulated in M19 while methylene blue molecules were trapped in the pores of the supramolecular gel at the same time. Methylene blue was released to water phase along with gel-sol transition caused by heating, with emodin remained inside M19, which could be released by adding excess acid to destroy M19. The controlled release of different cargos based on M19 will pave the way for the use of supramolecular materials in drug delivery and controlled release applications.

# 5 $\pi$ - $\pi$ stacking between MOCs

 $\pi$ - $\pi$  stacking is common between phenyl groups when they are close, with the sandwich and T-shaped interactions being energetically more favored than the parallel-displaced interaction (Fig. 14). It is often observed when the MOCs contain ligands with phenyl groups, e.g., TPE-based ligands.

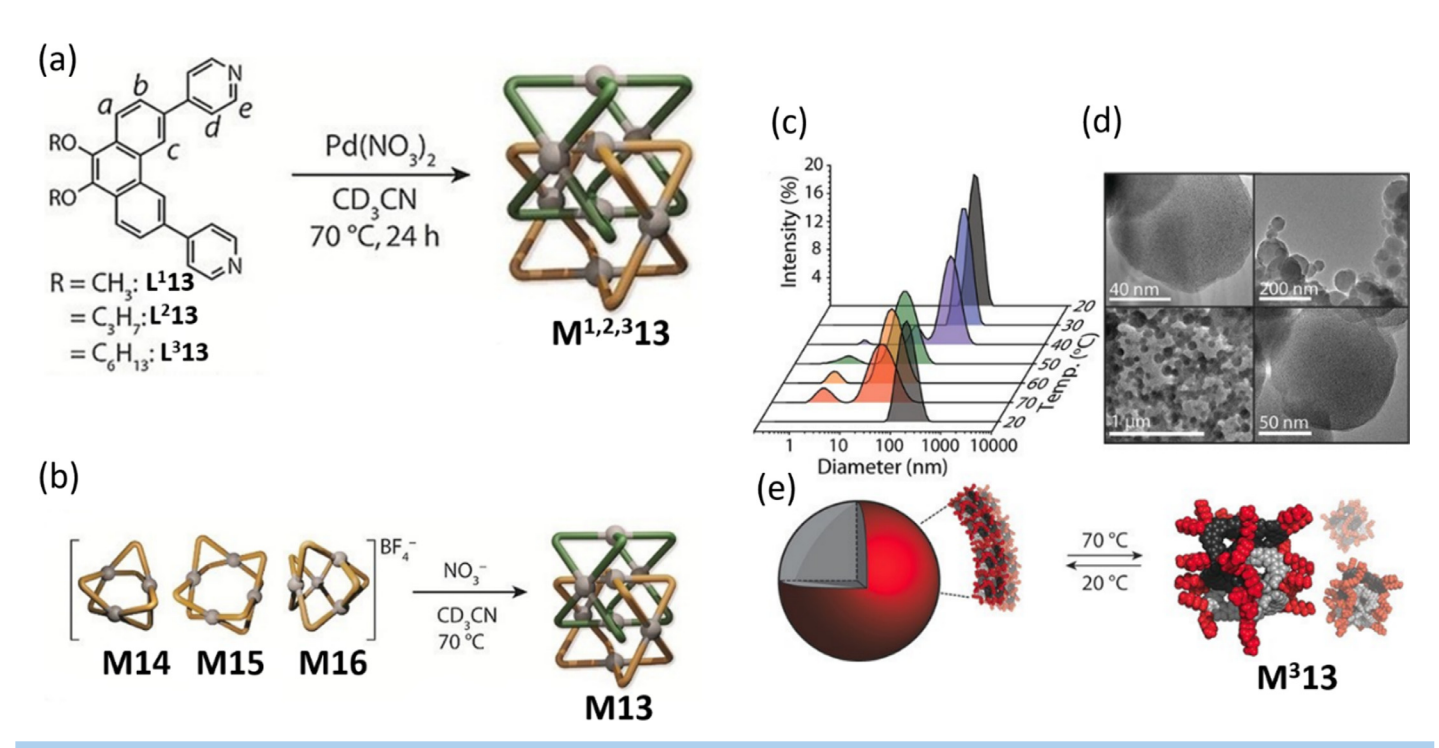


Fig. 10

(a) Synthesis of  $M^{1,2,3}13$  in one step using Pd(NO<sub>3</sub>)<sub>2</sub>. (b) Synthesis of M13 in two steps. First, obtaining M14, M15, and M16; then, treating them with Pd(NO<sub>3</sub>)<sub>2</sub> to obtain M13. (c) DLS size distribution results indicating that elevated temperatures lead to the disassembly of vesicular structures. (d) TEM images of the self-assembled vesicles. (e) Schematic representation of the thermoreversible assembly/disassembly process. Adapted with permission from ref 84. Copyright © 2018 Wiley-VCH.

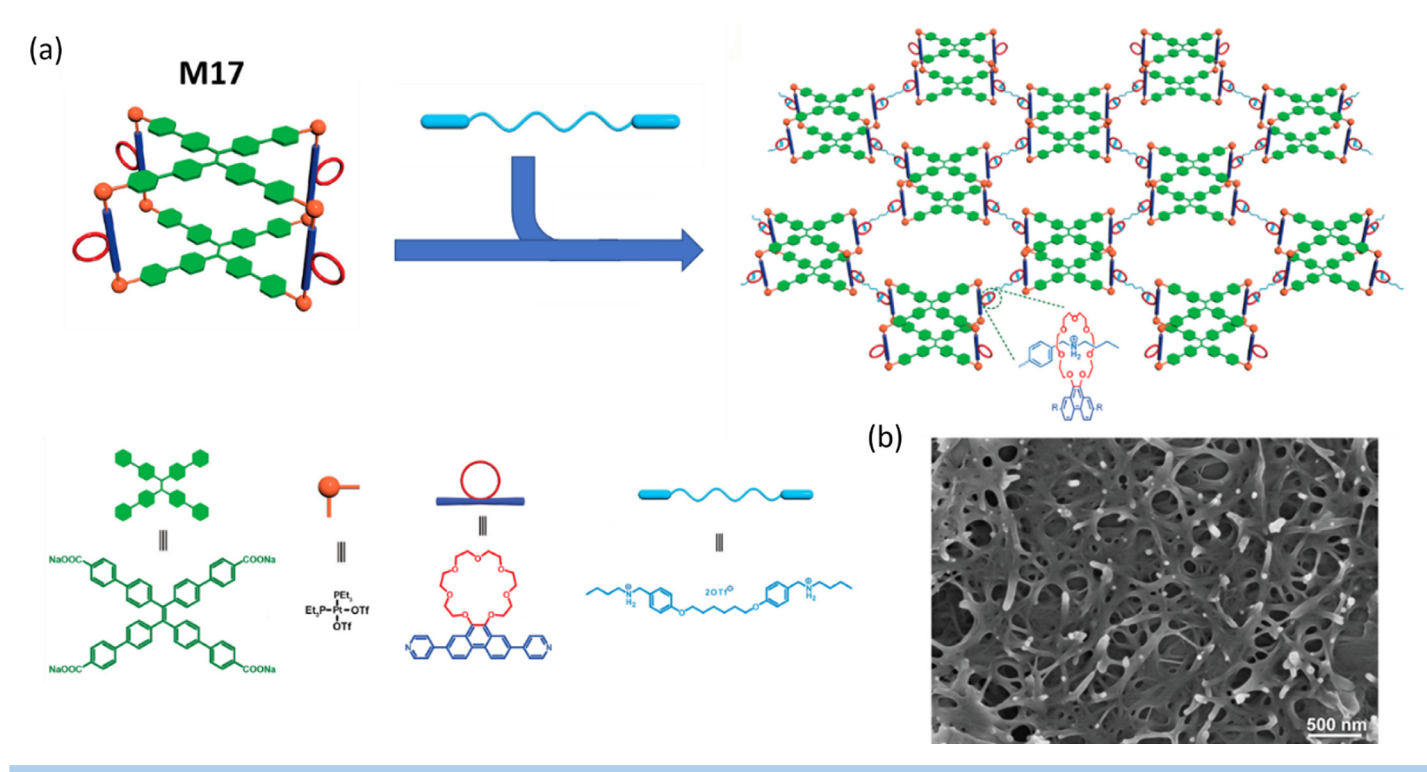


Fig. 11

(a) Molecular structure of **M17** and formation of cross-linked supramolecular structure from **M17** and bis-ammonium Salt. (b) SEM image of freeze-dried **M17**-based gel, scale bar: 500 nm. Adapted with permission from ref 86. Copyright 2018 American Chemical Society.

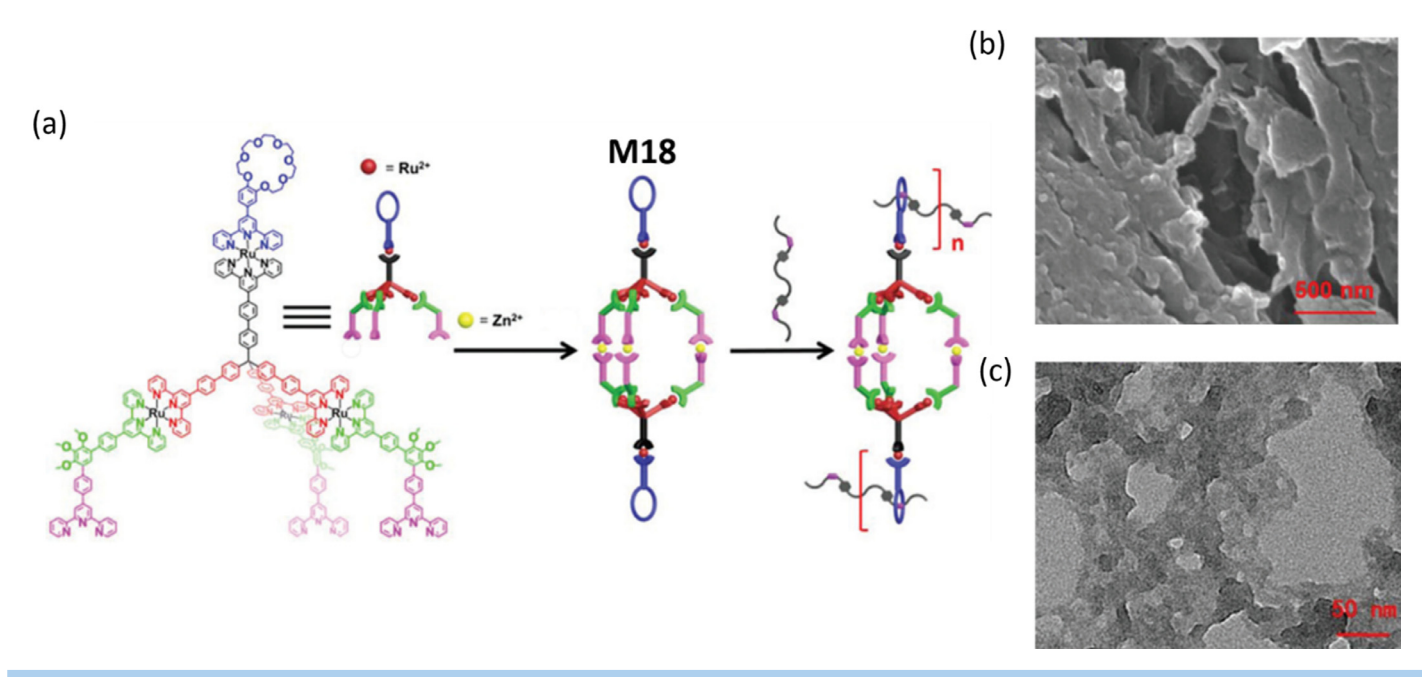


Fig. 12

(a) Molecular structure of **M18** and host-guest interactions with symmetrical difunctional alkylammonium salt. SEM (b) and TEM (c) images of gels formed by **M18** with addition of bis-ammonium salt. Adapted with permission from ref 87. Copyright © 2018, Royal Society of Chemistry.

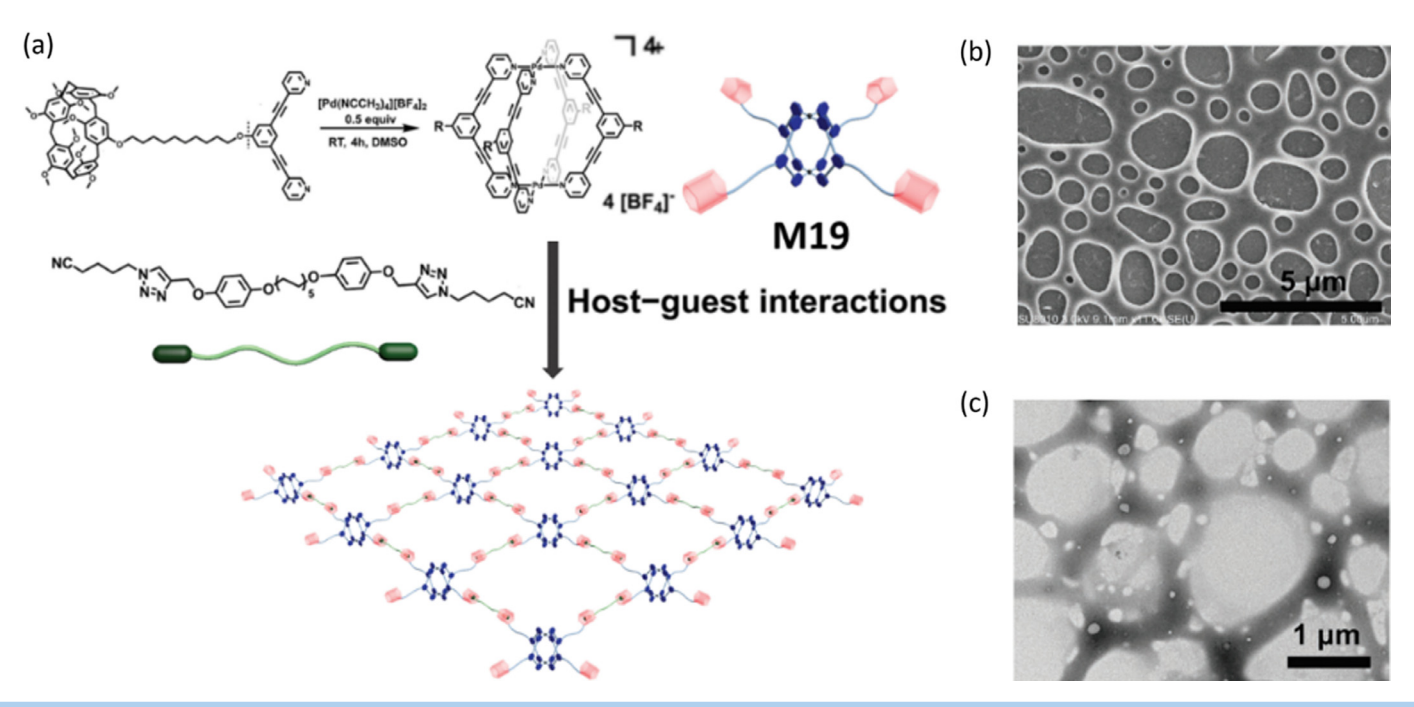


Fig. 13

(a) Molecular structure of **M19** and ditopic guest and cartoon representation of the formation or crosslinked supramolecular network. SEM image (b) and TEM image (c) of the interconnected porous structure formed by **M19** and ditopic guest in CHCl<sub>3</sub>. Scale bar: (b) 5  $\mu$ m and (c) 1  $\mu$ m. Adapted with permission from ref 89. Copyright © 2018 WILEY-VCH.

Introduction of TPPE in **M8** and the large conjugation area of the MOC offer the possibility of  $\pi-\pi$  interaction among MOCs. As mentioned earlier, cationic **M8** forms blackberry structures in ethyl acetate solution due to counterion-mediated attraction, whereas microneedles were obtained in a mixture

of dichloromethane and ethyl acetate, which further stacked together to produce microflowers during solvent evaporation [90]. The intermediates of multilamellar structures were detected, which gradually converted to microneedles, reveled the mechanism of microneedle formation by staking of thin

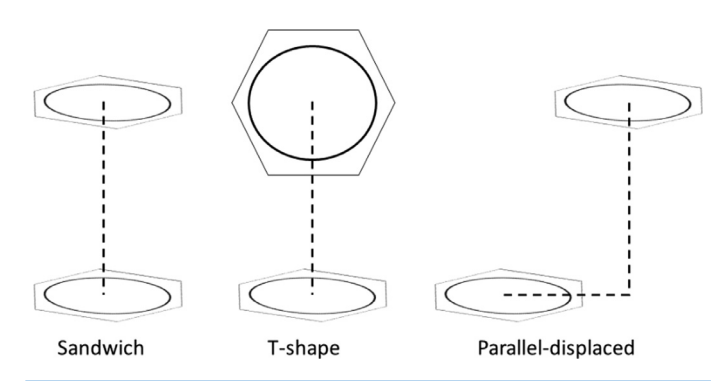


Fig. 14

Schematic showing  $\pi$ - $\pi$  stacking with sandwich, T-shape, and parallel-displaced conformations. Sandwich and T-shape conformations are favored due to lower energy.

layers. The discrete M8 dispersed in dichloromethane and stacked together via  $\pi - \pi$  interaction when ethyl acetate was introduced, forming elongated supramolecular structures, and further assembling into microneedles. However, the mechanism of the microflowers formation remains unclear. By changing the molar ratio of dichloromethane and ethyl acetate in the mixed solvent, the width and length of the microneedles increase with increasing ethyl acetate percentage. It is interesting to observe that diverse supramolecular structures were achieved based on the same MOC (M8) at different conditions (Fig. 15). The reason is that several intermolecular interactions can be endowed due to the introduction of various ligands within one MOC, making MOCs promising candidates for building up smart materials with different applications. Moreover, the introduction of biomolecules, both water-soluble vitamin B<sub>12</sub> and oil-soluble chlorophyll-a, into microneedles were achieved via simple physical adsorption, demonstrating the potential of MOC as artificial biological units for mimicking and optimizing assembly-based synthetic systems.

Changing the substituents within MOC can also lead to different nanostructures. Keeping the TPPEs and metal acceptors in M8, together with isophthalates modified with sodium sulfonate (L20), nitro (L21), methoxyl (L22), or amine groups (L23), as pillars, M20, M21, M22 and M23 were obtained, respectively (Fig. 16) [91]. **M20** assembles into microfibers in water which was driven by  $\pi$ - $\pi$  stacking of TPPE, whereas microspheres with diameters of tens of nanometers formed by the assembly of M20 in tetrahydrofuran. With nitro group-modified isophthalates (L21), M21 self-assembles into microplates in tetrahydrofuran, while microfilms, ranged from a few hundred nanometers to a few micrometers in size, were formed in ethanol. In tetrahydrofuran, M22, with methoxy groups linked with pillars (L23), assembles into hollow spheres, with diameters ranging from a few hundred nanometers to a few micrometers. When an amine groupmodified isophthalate (L23) used as a pillar, M23 self-assembles into microsheets in tetrahydrofuran. With slightly changing of side ligands, tunability of intermolecular interaction can be achieved and lead to various supramolecular structures. Their optical properties were tested and found to be closely related to the substituents, solvents and supramolecular structure formed. The broad emission range can be realized, laying the foundation for MOC-based optoelectronic materials.

If the phenyl groups are on the edge ligands or as the side groups, there would be more chances forming 2D or 3D network instead of 1D fibers. With twelve 180-degree Zn(II) ligands and eight 90-degree three-armed donors, **M24** was obtained [92]. In acetonitrile, **M24** forms hybrid gel when mixing with polypyrrole (PPy), revealing thin film structures which wrapped the PPy particles and further connects the PPy domains together (Fig. 17). The rigid and uniform geometry of **M24** enhances its hierarchical self-assembly and forms gels due to intermolecular interactions, such as hydrophobic interactions and  $\pi$ - $\pi$  stacking. The combination of PPy and **M24** supramolecular gel offers the system high conductivity and self-healing property, exhibiting excellent mechanical strength and elasticity and showing its

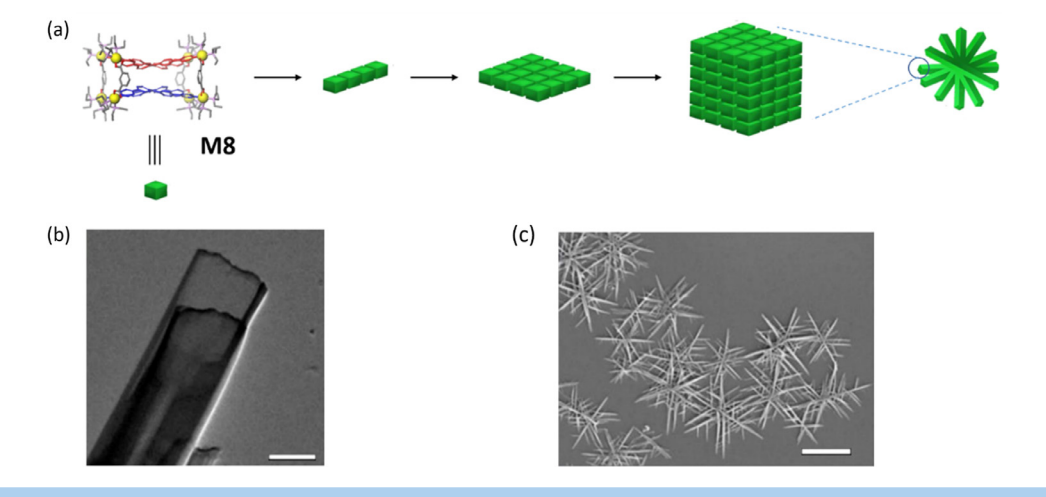


Fig. 15

(a) Schematic showing molecular structure of **M8** and its self-assembly in binary solvent of EA and DCM. (b) TEM images of microneedles formed by **M8** in a DCM/EA mixture with 80% EA, scale bar: 500 nm. (c) SEM image of microneedle-based microflowers form in a DCM/EA mixture with 80% EA, scale bar: 4  $\mu$ m. Adapted with permission from ref 90. Copyright 2018 American Chemical Society.

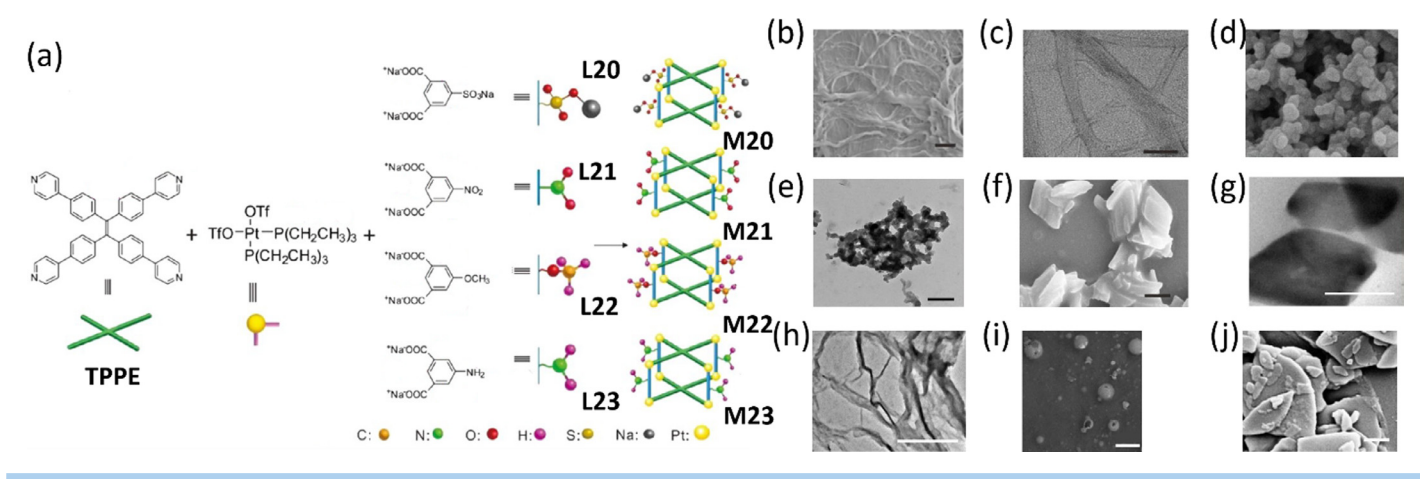


Fig. 16

(a) Molecular structure of **M20-M23**. SEM (b,d) and TEM (c,e) images of microfibers and microspheres formed by **M20** in water and THF, respectively, at scale bar:  $5 \mu m$ , 100 nm, 200 nm and 500 nm. SEM (f) and TEM (g,h) images of **M21**-based microplates in tetrahydrofuran and microfilms formed in ethanol at scale bar:  $1 \mu m$ ,  $0.5 \mu m$ , and  $1 \mu m$ , respectively. (i) SEM image of **M22**-based hollow microspheres, formed in THF at scale bar:  $2 \mu m$ . (j) SEM images of the micro-leaves formed by **M23** in tetrahydrofuran at scale bar:  $1 \mu m$ . Adapted with permission from ref 91. Copyright © 2018, American Chemical Society.

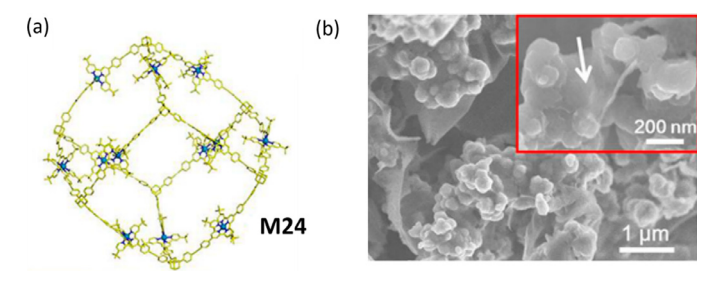


Fig. 17

(a) Molecular structure of **M24.** Blue: Zn(II) metal acceptors; yellow: 2,2':6',2'-terpyridine organic ligands. (b) SEM images of PPy/G-Zn-tpy hybrid gel, showing the nanosheet formed by **M24** and wrapped PPy nanoparticles. Adapted with permission from ref 92. Copyright 2015, American Chemical Society.

potential applications in many fields, such as self-healing electronics.

**M25** [57], with  $\pi$  system as side groups, is constructed by mixing alkynylplatinum(II) bzimpy-containing dipyridine ligand with Palladium acceptors (Fig. 18). **M25** can self-assemble into rodlike structures in a binary solution of DMF and water, and consequently lead to gelation. Presence of Pt as the coordination metal, and several phenyl groups in the ligand's structure make it obvious that Pt...Pt and  $\pi$ - $\pi$  stacking, imposed by alkynylplatinum(II) bzimpy, are the dominant intermolecular interactions.

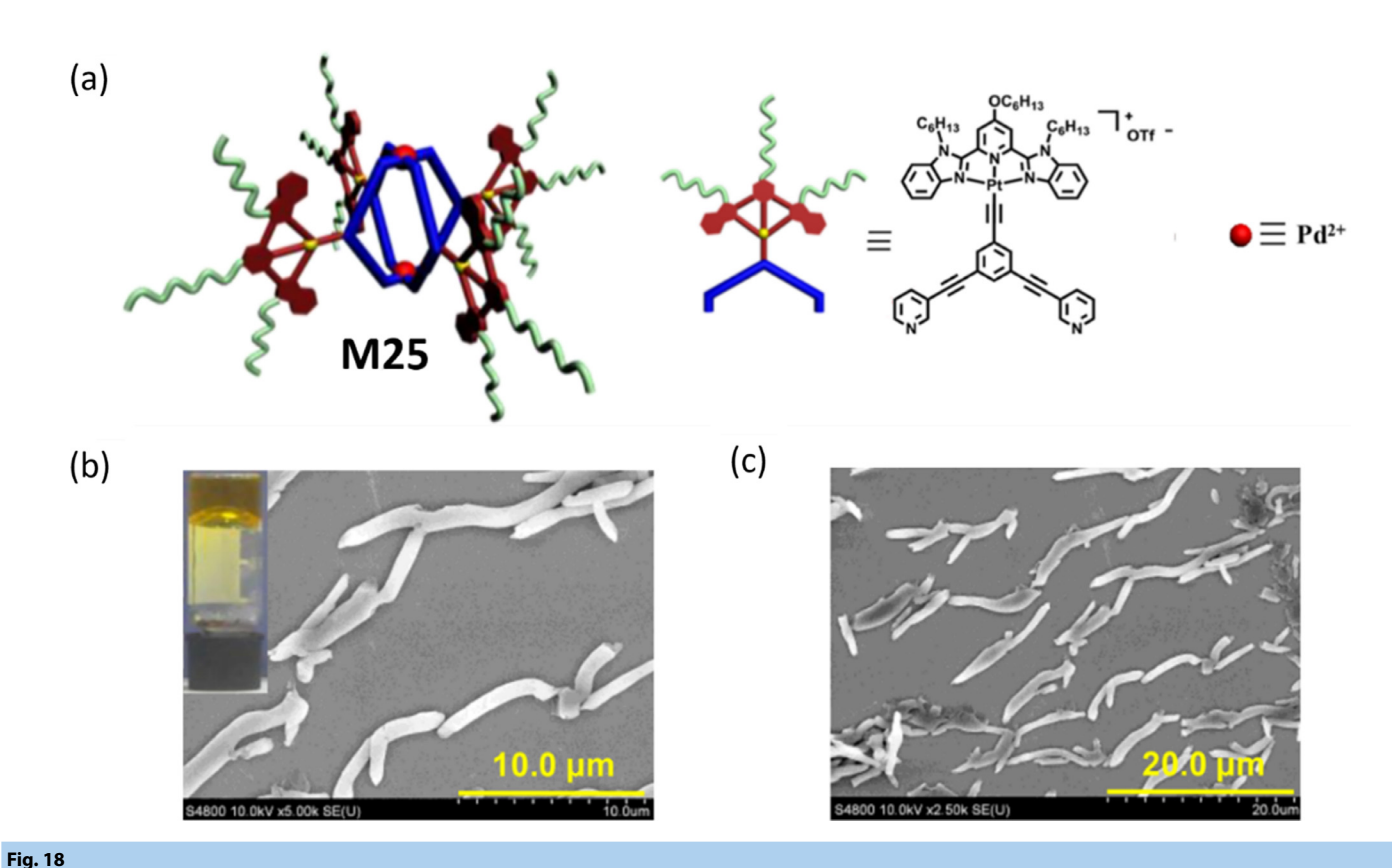
#### 6 Van der Waals interactions between MOCs

Van der Waals forces always exist among MOCs. They are weak interactions and will become dominant to regulate the self-assembly of MOCs often when other interactions are negligible. One example is cholesteryl covered  $Pd_{12}L_{24}$  (L is cholesteryl-functionalized 3,5-bis(4-pyridyl)benzene) (**M26**), which was synthesized to obtain a physical gel with sponge-like

porous network structures based on interconnected 20-50 nm sized nanoparticles in mixed CHCl<sub>3</sub>/CH<sub>3</sub>CN solvent and their deuterated counterparts (Fig. 19) [93]. In this system, M26 has been extensively covered so that the charges and functional groups on it do not contribute much to the inter-MOC interaction; meanwhile, in this weak polar solvent hydrophobic interaction is also very minor. Hence, van der Waals interactions between cholesteryl moieties become the key driving force of the selfassembly process. The gels were thermoreversible only when prepared in deuterated solvents. Rheological characterizations indicated that gels possess a predominant elastic behavior. Moreover, storage modulus (G) of gels in deuterated solvents was much lower than that in regular solvents, revealing that gelator is much weaker and softer in deuterated solvents resulting in gels with inferior mechanical properties. To prove the effectiveness of cholesteryl-cholesteryl interactions, 20% of the ligands with cholesteryl moieties (L26) were replaced with simple bipyridine ligands (L<sup>0</sup>26). Obtained gels by these MOCs with mixed ligands the lower number of cholesteryl moieties in the structure of cuboctahedra MOCs and weaker intermolecular interactions. Additionally, replacement of a TPE functionalized ligand in the MOCs offers the gels with tunable luminescence properties, which is anion responsive such as CN-. This study is a good example of a tunable responsible physical gels obtained by MOCs. Both mechanical and luminescence properties of the gels can be tuned by partial replacement of the cholesteryl ligands with other proper ligands.

#### 7 Hydrogen bonding between MOCs

As a directional, short-ranged interaction, hydrogen bonding can effectively control self-assembly processes of MOCs in polar solvents, especially water. Hydrogen bonding exhibits great thermoreversibility and specificity, allowing reversible interactions between MOCs and other molecules. In addition,



(a) Molecular structure of **M25**. SEM images (b,c) of xerogel formed by **M25**. Scale bar: (b) 10  $\mu$ m and (c) 20  $\mu$ m. Adapted with permission from ref 57. Copyright © 2018, American Chemical Society.

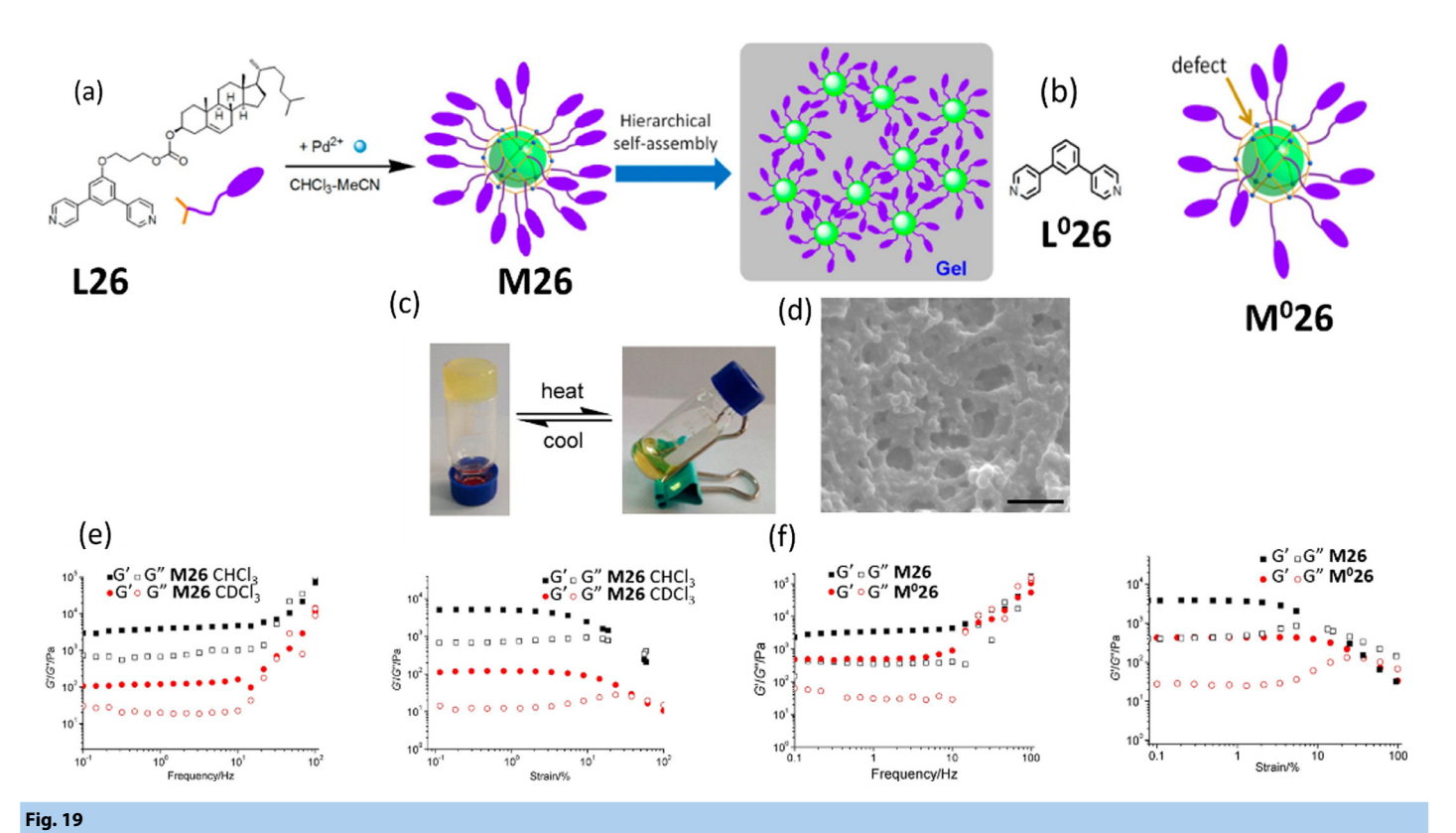
the tunability of hydrogen bonding strength can be achieved via changing hydrogen bonding sites. Taking Ga-based metal ligands as acceptors, together with 4,5-imidazoledicarboxylic acid (H<sub>3</sub>ImDC), a cubic MOC (M27, Fig. 20a) [94] was constructed. Introducing diverse molecular binders such as ammonium ion, N-(2-aminoethyl)-1,3-propanediamine (AEPD), guanidine hydrochloride (gua.HCl) or  $\beta$ -alanine ( $\beta$ -ala) into the aqueous solution of M27, hydrogels with nanotube, nanobouquet, nanosheet and nanocube as nanostructures, were observed as shown in Figs. 20b-e, respectively. With the addition of NH<sub>4</sub>+, the charge-assisted H-bonding between NH<sub>4</sub><sup>+</sup> and peripheral carboxylate oxygens of M27 facilitates the assembly of M27 and results in irregular crumpled sheets, which act as nodal points for further anisotropic growth towards the closely spaced 1D tapes and then formed nanotubes. Altering externally added molecular binders with H-donor sites, the morphology of the self-assembly nanostructures varied, indicating the structure, geometry, and number of H-bonding donor sites of molecular binders are important. This indicates that a simple replacement of binding molecules can greatly affect the inter-MOC interactions and the resulting supramolecular structures.

#### 8 Summary and concluding remarks

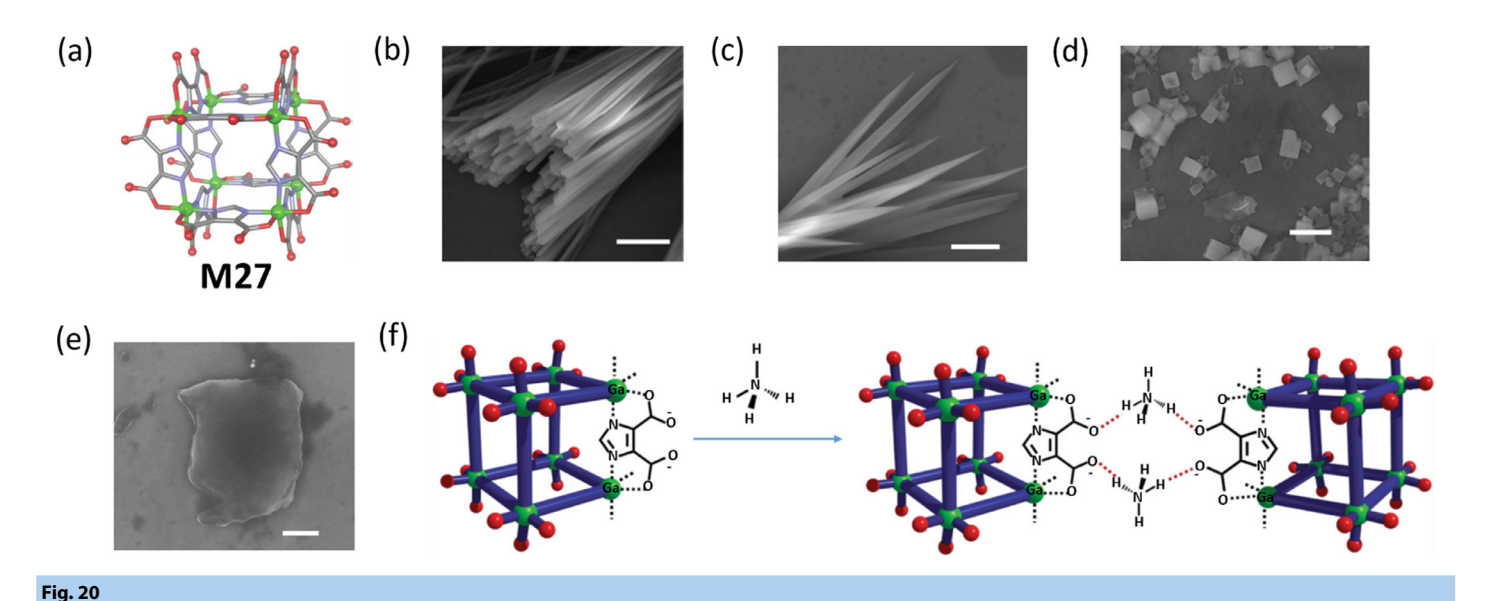
In summary, MOCs have unique features that make them exciting building blocks of supramolecular structures including their diverse and well-defined structure and geometry, confined

tunable cavity, diverse functionalities, and hybrid (organicinorganic) properties. All these features help generating different physical intermolecular interactions with tunable strengths, such as electrostatic, hydrophobic, hydrogen bonding,  $\pi$ - $\pi$  stacking, *etc.*, bringing MOCs together to self-assemble into a large variety of nanostructures.

The presence of metal acceptors (or even charged ligands) endows macroionic properties to the MOCs which introduce electrostatic interaction as one of the important intermolecular interactions during their self-assembly. Besides, functionalization of the ligands can possibly offer MOCs other interactions such van der Waals, host-guest, hydrophobic, H-bonding, etc. Exceptional tunability of MOCs enables the formation of different supramolecular structures with various functions, such as structures with tunable and responsive fluorescence or capability of controllable drug release. Besides, tiny variations in the substituents of MOCs, changing solvent composition, tuning surface charge of MOCs, or even simply changing the binding molecules (if any) can significantly change the properties of the supramolecular structures such as size, luminescence, mechanical properties, and the type of supramolecular structures. Moreover, structural complexity and tunability of MOCs can help us to mimic naturally occurring self-assembly processes to possibly find answers to many fundamental scientific questions such as the origin of homochirality, or the mechanism behind a DNA condensation process.



(a) Structure of **M26** and its ligand (**L26**). (b) Structure of the cuboctahedron cage with mixed ligand **M<sup>0</sup>26** in which **L<sup>0</sup>26** is used along with **L26**. (c) Thermoreversibility of gels in deuterated solvent. (d) SEM image of the interconnected structure of gel. (e) Storage (G) and loss (G") moduli of gels formed by **M26** in CHCl<sub>3</sub> and CDCl<sub>3</sub> in frequency sweep (left) and strain sweep (right) tests. Higher G' can be observed for gels formed in CHCl<sub>3</sub>. (f) G' and G" of **M26** and **M<sup>0</sup>26** in both frequency sweep (left) and strain sweep (right) rheological tests. Adapted with permission from ref 93. Copyright © 2019, American Chemical Society.



(a) Molecular tructure of MOC **M27**. Red: oxygen; blue: nitrogen; green: Gallium; gray: carbon. Field emission scanning electron microscope (FESEM) images of hydrogels formed by **M27** with addition of (b) ammonium ion (scale bar: 2  $\mu$ m), (c) AEPD (scale bar: 2  $\mu$ m), (d) gua.HCl (scale bar: 500 nm) and (d)  $\beta$ -ala (scale bar: 1  $\mu$ m), respectively. (f) Scheme showing the charge-assisted H-bonding interaction between **M27** and ammonium ions. Adapted with permission from ref 94. Copyright 2018, Papri Sutar, et al.

### **Declaration of Competing Interest**

The authors declare that they have no known competing financial interests or personal relationships that could have appeared to influence the work reported in this paper.

# **Acknowledgments**

T.L. acknowledges support from the National Science Foundation (CHE1904397) and The University of Akron.

#### References

- G.A. Lawrance, Introduction to Coordination Chemistry, Wiley, 2013. https://books.google.com/books?id=40NWXyI7DskC.
- [2] S. Datta, M.L. Saha, P.J. Stang, Hierarchical assemblies of supramolecular coordination complexes, Acc. Chem. Res. 51 (2018) 2047–2063, doi:10.1021/acs. accounts.8b00233.
- [3] R. Chakrabarty, P.S. Mukherjee, P.J. Stang, Supramolecular coordination: self-assembly of finite two- and three-dimensional ensembles, Chem. Rev. 111 (2011) 6810–6918, doi:10.1021/cr200077m.
- [4] K. Harris, D. Fujita, M. Fujita, Giant hollow  $M_nL_{2n}$  spherical complexes: structure, functionalisation and applications, Chem. Commun. 49 (2013) 6703–6712, doi:10.1039/C3CC43191F.
- [5] M. Fujita, M. Tominaga, A. Hori, B. Therrien, Coordination assemblies from a Pd(II)-cornered square complex, Acc. Chem. Res. 38 (2005) 369–378, doi:10.1021/ ar040153h.
- [6] T.R. Cook, P.J. Stang, Recent developments in the preparation and chemistry of metallacycles and metallacages via coordination, Chem. Rev. 115 (2015) 7001– 7045, doi:10.1021/cr5005666.
- [7] P.J. Stang, B. Olenyuk, Self-assembly, symmetry, and molecular architecture: coordination as the motif in the rational design of supramolecular metallacyclic polygons and polyhedra, Acc. Chem. Res. 30 (1997) 502–518, doi:10.1021/ ar9602011.
- [8] I. Eryazici, C.N. Moorefield, G.R. Newkome, Square-planar Pd(II), Pt(II), and Au(III) terpyridine complexes: their syntheses, physical properties, supramolecular constructs, and biomedical activities, Chem. Rev. 108 (2008) 1834–1895, doi:10.1021/cr0781059.
- [9] M.M.J. Smulders, I.A. Riddell, C. Browne, J.R. Nitschke, Building on architectural principles for three-dimensional metallosupramolecular construction, Chem. Soc. Rev. 42 (2013) 1728–1754, doi:10.1039/C2CS35254K.
- [10] J.R. Nitschke, Construction, substitution, and sorting of metallo-organic structures via subcomponent self-assembly, Acc. Chem. Res. 40 (2007) 103–112, doi:10.1021/ar068185n.
- [11] Z. Zhou, D.-.G. Chen, M.L. Saha, H. Wang, X. Li, P.-.T. Chou, P.J. Stang, Designed conformation and fluorescence properties of self-assembled phenazine-cored platinum(II) metallacycles, J. Am. Chem. Soc. 141 (2019) 5535–5543, doi:10. 1021/jacs.9b01368.
- [12] X. Chang, Z. Zhou, C. Shang, G. Wang, Z. Wang, Y. Qi, Z.-Y. Li, H. Wang, L. Cao, X. Li, Y. Fang, P.J. Stang, Coordination-driven self-assembled metallacycles incorporating pyrene: fluorescence mutability, tunability, and aromatic amine sensing, J. Am. Chem. Soc. 141 (2019) 1757–1765, doi:10.1021/jacs.8b12749.
- [13] A. Garci, K.J. Castor, J. Fakhoury, J.-.L. Do, J. Di Trani, P. Chidchob, R.S. Stein, A.K. Mittermaier, T. Friščić, H. Sleiman, Efficient and rapid mechanochemical assembly of platinum(II) squares for guanine quadruplex targeting, J. Am. Chem. Soc. 139 (2017) 16913–16922, doi:10.1021/jacs.7b09819.
- [14] G.-.F. Huo, X. Shi, Q. Tu, Y.-.X. Hu, G.-.Y. Wu, G.-.Q. Yin, X. Li, L. Xu, H.-.M. Ding, H.-.B. Yang, Radical-induced hierarchical self-assembly involving supramolecular coordination complexes in both solution and solid states, J. Am. Chem. Soc. 141 (2019) 16014–16023, doi:10.1021/jacs.9b08149.
- [15] Y. Sun, F. Ding, Z. Chen, R. Zhang, C. Li, Y. Xu, Y. Zhang, R. Ni, X. Li, G. Yang, Y. Sun, P.J. Stang, Melanin-dot-mediated delivery of metallacycle for NIR-II/photoacoustic dual-modal imaging-guided chemo-photothermal synergistic therapy, Proc. Natl. Acad. Sci. 116 (2019) 16729 LP 16735, doi:10.1073/pnas. 1908761116.
- [16] A.J. Musser, P.P. Neelakandan, J.M. Richter, H. Mori, R.H. Friend, J.R. Nitschke, Excitation energy delocalization and transfer to guests within  $M^{II}_{4}L_{6}$  cage frameworks, J. Am. Chem. Soc. 139 (2017) 12050–12059, doi:10.1021/jacs. 7b06709.
- [17] B.S. Pilgrim, D.A. Roberts, T.G. Lohr, T.K. Ronson, J.R. Nitschke, Signal transduction in a covalent post-assembly modification cascade, Nat. Chem. 9 (2017) 1276–1281, doi:10.1038/nchem.2839.
- [18] I.M. Müller, S. Spillmann, H. Franck, R. Pietschnig, Rational design of the first closed coordination capsule with octahedral outer shape, Chem. A Eur. J. 10 (2004) 2207–2213, doi:10.1002/chem.200305564.
- [19] Q.-.F. Sun, S. Sato, M. Fujita, An  $M_{18}L_{24}$  stellated cuboctahedron through post-stellation of an  $M_{12}L_{24}$  core, Nat. Chem. 4 (2012) 330–333, doi:10.1038/nchem. 1285.

- [20] N. Liu, T. Lin, M. Wu, H.-.K. Luo, S.-.L. Huang, T.S.A. Hor, Suite of organoplatinum(II) triangular metallaprism: aggregation-induced emission and coordination sequence induced emission tuning, J. Am. Chem. Soc. 141 (2019) 9448–9452, doi:10.1021/jacs.9b01283.
- [21] J.Y. Ryu, J.M. Lee, N. Van Nghia, K.M. Lee, S. Lee, M.H. Lee, P.J. Stang, J. Lee, Supramolecular Pt(II) and Ru(II) trigonal prismatic cages constructed with a tris(pyridyl)borane donor, Inorg. Chem. 57 (2018) 11696–11703, doi:10.1021/ acs.inorgchem.8b01830.
- [22] G. Yu, Y. Ye, Z. Tong, J. Yang, Z. Li, B. Hua, L. Shao, S. Li, A porphyrin-based discrete tetragonal prismatic cage: host–guest complexation and its application in tuning liquid-crystalline behavior, Macromol. Rapid Commun. 37 (2016) 1540– 1547, doi:10.1002/marc.201600280.
- [23] G. Yu, B. Zhu, L. Shao, J. Zhou, M.L. Saha, B. Shi, Z. Zhang, T. Hong, S. Li, X. Chen, P.J. Stang, Host–guest complexation-mediated codelivery of anticancer drug and photosensitizer for cancer photochemotherapy, Proc. Natl. Acad. Sci. 116 (2019) 6618 LP – 6623, doi:10.1073/pnas.1902029116.
- [24] C.J. Brown, F.D. Toste, R.G. Bergman, K.N. Raymond, Supramolecular catalysis in metal-ligand cluster hosts, Chem. Rev. 115 (2015) 3012–3035, doi:10.1021/ cr4001226.
- [25] Q.-.Q. Wang, S. Gonell, S.H.A.M. Leenders, M. Dürr, I. Ivanović-Burmazović, J.N.H. Reek, Self-assembled nanospheres with multiple endohedral binding sites pre-organize catalysts and substrates for highly efficient reactions, Nat. Chem. 8 (2016) 225, doi:10.1038/nchem.2425.
- [26] K.M.L. Taylor-Pashow, J. Della Rocca, Z. Xie, S. Tran, W. Lin, Postsynthetic modifications of iron-carboxylate nanoscale metal—organic frameworks for imaging and drug delivery, J. Am. Chem. Soc. 131 (2009) 14261–14263, doi:10. 1021/ja906198y.
- [27] D. Zhao, S. Tan, D. Yuan, W. Lu, Y.H. Rezenom, H. Jiang, L.-.Q. Wang, H.-.C. Zhou, Surface functionalization of porous coordination nanocages via click chemistry and their application in drug delivery, Adv. Mater. 23 (2011) 90–93, doi:10.1002/ adma.201003012.
- [28] S. Qiu, G. Zhu, Molecular engineering for synthesizing novel structures of metalorganic frameworks with multifunctional properties, Coord. Chem. Rev. 253 (2009) 2891–2911, doi:10.1016/j.ccr.2009.07.020.
- [29] M. Zhang, M.L. Saha, M. Wang, Z. Zhou, B. Song, C. Lu, X. Yan, X. Li, F. Huang, S. Yin, P.J. Stang, Multicomponent platinum(II) Cages with tunable emission and amino acid sensing, J. Am. Chem. Soc. 139 (2017) 5067–5074, doi:10.1021/jacs. 6b12536.
- [30] Y. Sun, C. Chen, J. Liu, P.J. Stang, Recent developments in the construction and applications of platinum-based metallacycles and metallacages via coordination, Chem. Soc. Rev. 49 (2020) 3889–3919, doi:10.1039/D0CS00038H.
- [31] J.N. Israelachvili, D.J. Mitchell, B.W. Ninham, Theory of self-assembly of lipid bilayers and vesicles, Biochim. Biophys. Acta Biomembr. 470 (1977) 185–201, doi:10.1016/0005-2736(77)90099-2.
- [32] H. Noguchi, G. Gompper, Dynamics of vesicle self-assembly and dissolution, J. Chem. Phys. 125 (2006) 164908, doi:10.1063/1.2358983.
- [33] J. Luo, S. Ye, P. Ustriyana, B. Wei, J. Chen, E. Raee, Y. Hu, Y. Yang, Y. Zhou, C. Wesdemiotis, N. Sahai, T. Liu, Unraveling chiral selection in the self-assembly of chiral fullerene macroions: effects of small chiral components including counterions, co-ions, or neutral molecules, Langmuir 36 (2020) 4702–4710, doi:10.1021/acs.langmuir.0c00611.
- [34] J.W. Steed, J.L. Atwood, Supramolecular Chemistry, Wiley, 2013. https://books.google.com/books?id=8G3kGIoAkaQC.
- [35] J. Luo, X. Sun, J.--F. Yin, P. Yin, T. Liu, Supramolecular nanostructures constructed from cluster-based hybrid macromolecules, Giant 2 (2020) 100013, doi:10.1016/ j.giant.2020.100013.
- [36] S. Jana, M. de Frutos, P. Davidson, B. Abécassis, Ligand-induced twisting of nanoplatelets and their self-assembly into chiral ribbons, Sci. Adv. 3 (2017) e1701483. doi:10.1126/sciadv.1701483.
- [37] C. Lara, J. Adamcik, S. Jordens, R. Mezzenga, General self-assembly mechanism converting hydrolyzed globular proteins into giant multistranded amyloid ribbons, Biomacromolecules 12 (2011) 1868–1875, doi:10.1021/bm200216u.
- [38] A.H. Gröschel, F.H. Schacher, H. Schmalz, O.V. Borisov, E.B. Zhulina, A. Walther, A.H.E. Müller, Precise hierarchical self-assembly of multicompartment micelles, Nat. Commun. 3 (2012) 710, doi:10.1038/ncomms1707.
- [39] J.N. Israelachvili, D.J. Mitchell, B.W. Ninham, Theory of self-assembly of hydrocarbon amphiphiles into micelles and bilayers, J. Chem. Soc. Faraday Trans. 2 Mol. Chem. Phys. 72 (1976) 1525–1568, doi:10.1039/F29767201525.
- [40] A. Ulman, An Introduction to Ultrathin Organic Films: From Langmuir-Blodgett to Self-Assembly, Elsevier Science, 2013. https://books.google.com/books?id= 4qb8BAAAQBAJ.
- [41] G.D. Pins, D.L. Christiansen, R. Patel, F.H. Silver, Self-assembly of collagen fibers. Influence of fibrillar alignment and decorin on mechanical properties, Biophys. J. 73 (1997) 2164–2172, doi:10.1016/S0006-3495(97)78247-X.
- [42] D.E. Przybyla, J. Chmielewski, Metal-triggered radial self-assembly of collagen peptide fibers, J. Am. Chem. Soc. 130 (2008) 12610–12611, doi:10.1021/ ia804942w
- [43] T. Liu, E. Diemann, H. Li, A.W.M. Dress, A. Müller, Self-assembly in aqueous

- solution of wheel-shaped Mo<sub>154</sub> oxide clusters into vesicles, Nature 426 (2003) 59–62, doi:10.1038/nature02036.
- [44] J. Luo, T. Liu, Competition and cooperation among different attractive forces in solutions of inorganic-organic hybrids containing macroionic clusters, Langmuir 35 (2019) 7603–7616, doi:10.1021/acs.langmuir.9b00480.
- [45] F. Haso, J. Luo, B.S. Bassil, B. Artetxe, J. Zhou, P. Yin, S. Reinoso, J.M. Gutiérrez-Zorrilla, U. Kortz, T. Liu, Effect of directional hydrogen bonding on the self-assembly of anisotropically-shaped macroions, Chem. Select 1 (2016) 4345–4349, doi:10.1002/slct.201601154.
- [46] O.I. Nonappa, Hydrogen bonding directed colloidal self-assembly of nanoparticles into 2D crystals, capsids, and supracolloidal assemblies, Adv. Funct. Mater. 28 (2018) 1704328, doi:10.1002/adfm.201704328.
- [47] K. Tahara, S. Lei, J. Adisoejoso, S. De Feyter, Y. Tobe, Supramolecular surface-confined architectures created by self-assembly of triangular phenylene– ethynylene macrocycles via van der Waals interaction, Chem. Commun. 46 (2010) 8507–8525, doi:10.1039/C0CC02780D.
- [48] M. Dong, K. Miao, Y. Hu, J. Wu, J. Li, P. Pang, X. Miao, W. Deng, Cooperating dipole-dipole and van der Waals interactions driven 2D self-assembly of fluorenone derivatives: ester chain length effect, Phys. Chem. Chem. Phys. 19 (2017) 31113–31120, doi:10.1039/C7CP06462D.
- [49] Z. Shen, T. Wang, M. Liu, H-bond and π-π stacking directed self-assembly of two-component supramolecular nanotubes: tuning length, diameter and wall thickness, Chem. Commun. 50 (2014) 2096–2099, doi:10.1039/C3CC48350A.
- [50] K. Balakrishnan, A. Datar, W. Zhang, X. Yang, T. Naddo, J. Huang, J. Zuo, M. Yen, J.S. Moore, L. Zang, Nanofibril self-assembly of an arylene ethynylene macrocycle, J. Am. Chem. Soc. 128 (2006) 6576–6577, doi:10.1021/ja0618550.
- [51] P. Yin, P. Wu, Z. Xiao, D. Li, E. Bitterlich, J. Zhang, P. Cheng, D.V. Vezenov, T. Liu, Y. Wei, A double-tailed fluorescent surfactant with a hexavanadate cluster as the head group, Angew. Chem. Int. Ed. 50 (2011) 2521–2525, doi:10.1002/anie. 201006144.
- [52] D. Li, J. Song, P. Yin, S. Simotwo, A.J. Bassler, Y. Aung, J.E. Roberts, K.I. Hardcastle, C.L. Hill, T. Liu, Inorganic-organic hybrid vesicles with counterion- and pHcontrolled fluorescent properties, J. Am. Chem. Soc. 133 (2011) 14010–14016, doi:10.1021/ja204034g.
- [53] J. Chen, K. Qian, K. Xiao, J. Luo, H. Li, T. Ma, U. Kortz, M. Tsige, T. Liu, Co-ion effects in the self-assembly of macroions: from co-ions to co-macroions and to the unique feature of self-recognition, Langmuir 36 (2020) 10519–10527, doi:10. 1021/acs.langmuir.0c01797.
- [54] G. Liu, T. Liu, S.S. Mal, U. Kortz, Wheel-Shaped Polyoxotungstate  $[Cu_{20}Cl(OH)_{24}(H_2O)_{12}(P_8W_{48}O_{184})]_{25} \text{macroanions} \quad \text{form} \quad \text{supramolecular} \\ \text{"Blackberry" structure in aqueous solution, J. Am. Chem. Soc. 128 (2006)} \\ 10103-10110, \ \text{doi:} \frac{10.1021}{ja0610840}.$
- [55] M.L. Kistler, A. Bhatt, G. Liu, D. Casa, T. Liu, A complete macroion—"Blackberry" assembly—macroion transition with continuously adjustable assembly sizes in [Mo<sub>132</sub>] water/acetone systems, J. Am. Chem. Soc. 129 (2007) 6453–6460, doi:10. 1021/ja0685809.
- [56] D. Li, J. Zhang, K. Landskron, T. Liu, Spontaneous self-assembly of metal—organic cationic nanocages to form monodisperse hollow vesicles in dilute solutions, J. Am. Chem. Soc. 130 (2008) 4226–4227, doi:10.1021/ja710820a.
- [57] Y. Zhang, Q.-.F. Zhou, G.-.F. Huo, G.-.Q. Yin, X.-.L. Zhao, B. Jiang, H. Tan, X. Li, H.-.B. Yang, Hierarchical self-assembly of an alkynylplatinum(II) bzimpy-functionalized metallacage via Pt•••Pt and π-π interactions, Inorg. Chem. 57 (2018) 3516–3520, doi:10.1021/acs.inorgchem.7b02777.
- [58] N. Kamiya, M. Tominaga, S. Sato, M. Fujita, Saccharide-coated  $M_{12}L_{24}$  molecular spheres that form aggregates by multi-interaction with proteins, J. Am. Chem. Soc. 129 (2007) 3816–3817, doi:10.1021/ja0693082.
- [59] K. Harris, D. Fujita, M. Fujita, Giant hollow MnL<sub>2</sub>n spherical complexes: struct(1) Harris, K.; Fujita, D.; Fujita, M. Giant Hollow M<sub>n</sub>L<sub>2n</sub> spherical complexes: structure, functionalisation and applications, Chem. Commun. 49 (60) (2013) 6703–6712 ure, fun, Chem. Commun. 49 (2013) 6703–6712. 10.1039/C3CC43191F, doi:10.1039/C3CC43191F.
- [60] K. Suzuki, M. Kawano, S. Sato, M. Fujita, Endohedral peptide lining of a self-assembled molecular sphere to generate chirality-confined hollows, J. Am. Chem. Soc. 129 (2007) 10652–10653, doi:10.1021/ja073629b.
- [61] S. De, K. Mahata, M. Schmittel, Metal-coordination-driven dynamic heteroleptic architectures, Chem. Soc. Rev. 39 (2010) 1555–1575, doi:10.1039/B922293F.
- [62] L. Cao, P. Wang, X. Miao, Y. Dong, H. Wang, H. Duan, Y. Yu, X. Li, P.J. Stang, Diamondoid supramolecular coordination frameworks from discrete adamantanoid platinum(II) cages, J. Am. Chem. Soc. 140 (2018) 7005–7011, doi:10.1021/jacs.8b03856.
- [63] P. Debye, E. Hückel, De la theorie des electrolytes. I. abaissement du point de congelation et phenomenes associes, Phys. Z. 24 (1923) 185–206.
- [64] E.J.W. Venvey, J.T.G. Overbeek, Theory of the Stability of Lyophobic Colloids, Cour. Corpora-Tion, 1948.
- [65] J. Luo, S. Ye, T. Li, E. Sarnello, H. Li, T. Liu, Distinctive trend of metal binding affinity via hydration shell breakage in nanoconfined cavity, J. Phys. Chem. C 123 (2019) 14825–14833, doi:10.1021/acs.jpcc.9b03004.
- [66] J. Chen, Y. Ma, D. Zhang, Y. Yang, M.K. Bera, J. Luo, E. Raee, T. Liu, Ion-pairs of

- structurally related polyoxotantalate clusters and divalent metal cations, J. Coord. Chem. (2020), doi:10.1080/00958972.2020.1830073.
- [67] J. Chen, M.K. Bera, H. Li, Y. Yang, X. Sun, J. Luo, J. Baughman, C. Liu, X. Yao, S.S.C. Chuang, T. Liu, Accurate determination of the quantity and spatial distribution of counterions around a spherical macroion, Angew. Chem. Int. (2020) Ed. n/a, doi:10.1002/anie.202013806.
- [68] P. Yin, D. Li, T. Liu, Solution behaviors and self-assembly of polyoxometalates as models of macroions and amphiphilic polyoxometalate–organic hybrids as novel surfactants, Chem. Soc. Rev. 41 (2012) 7368–7383, doi:10.1039/C2CS35176E.
- [69] T. Liu, B. Imber, E. Diemann, G. Liu, K. Cokleski, H. Li, Z. Chen, A. Müller, Deprotonations and charges of well-defined {Mo<sub>72</sub>Fe<sub>30</sub>} nanoacids simply stepwise tuned by pH allow control/variation of related self-assembly processes, J. Am. Chem. Soc. 128 (2006) 15914–15920, doi:10.1021/ja066133n.
- [70] D. Li, W. Zhou, K. Landskron, S. Sato, C.J. Kiely, M. Fujita, T. Liu, Viral-capsid-type vesicle-like structures assembled from M<sub>12</sub>L<sub>24</sub> metal-organic hybrid nanocages, Angew. Chem. Int. Ed. 50 (2011) 5182–5187, doi:10.1002/anie.201007829.
- [71] A.A. Verhoeff, M.L. Kistler, A. Bhatt, J. Pigga, J. Groenewold, M. Klokkenburg, S. Veen, S. Roy, T. Liu, W.K. Kegel, Charge regulation as a stabilization mechanism for shell-like assemblies of polyoxometalates, Phys. Rev. Lett. 99 (2007) 66104, doi:10.1103/PhysRevLett.99.066104.
- [72] H. Li, J. Luo, T. Liu, Modification of the solution behavior of Pd<sub>12</sub>L<sub>24</sub> metalorganic nanocages via PEGylation, Chem. A Eur. J. 22 (2016) 17949–17952, doi:10.1002/chem.201604427.
- [73] E. Raee, H. Li, X. Sun, P. Ustriyana, J. Luo, J. Chen, N. Sahai, T. Liu, Strong enantiomeric preference on the macroion–counterion interaction induced by weakly associated chiral counterions, J. Phys. Chem. B 124 (2020) 9958–9966, doi:10.1021/acs.jpcb.0c07424.
- [74] H. Li, R. Wang, Y. Hong, Z. Liang, Y. Shen, Y. Nishiyama, T. Miyoshi, T. Liu, Tuning the intercage distance in charge-regulated blackberry-type assemblies through host–guest chemistry, Chem. A Eur. J. 25 (2019) 5803–5808, doi:10.1002/chem. 201900800.
- [75] X. Yan, T.R. Cook, P. Wang, F. Huang, P.J. Stang, Highly emissive platinum(II) metallacages, Nat. Chem. 7 (2015) 342–348, doi:10.1038/nchem.2201.
- [76] H. Li, T.-.Z. Xie, Z. Liang, Y. Shen, X. Sun, Y. Yang, T. Liu, Adjusting emission wavelength by tuning the intermolecular distance in charge-regulated supramolecular assemblies, J. Phys. Chem. C 123 (2019) 23280–23286, doi:10. 1021/acs.jpcc.9b08186.
- [77] M. Chen, J. Wang, D. Liu, Z. Jiang, Q. Liu, T. Wu, H. Liu, W. Yu, J. Yan, P. Wang, Highly stable spherical metallo-capsule from a branched hexapodal terpyridine and its self-assembled berry-type nanostructure, J. Am. Chem. Soc. 140 (2018) 2555–2561, doi:10.1021/jacs.7b10707.
- [78] Y. Yang, P. Rehak, T.-.Z. Xie, Y. Feng, X. Sun, J. Chen, P. Kral, T. Liu, Nanosheets and Hydrogels Formed By 2Nm Metal-Organic Cages with Electrostatic Interaction, ACS AMI, 2020, doi:10.1021/acsami.0c16366.
- [79] T. Kikuchi, S. Sato, D. Fujita, M. Fujita, Stepwise DNA condensation by a histone-mimic peptide-coated M<sub>12</sub>L<sub>24</sub> spherical complex, Chem. Sci. 5 (2014) 3257–3260, doi:10.1039/C4SC00656A.
- [80] Z. Zhang, Z. Zhao, Y. Hou, H. Wang, X. Li, G. He, M. Zhang, Aqueous platinum(II)-cage-based light-harvesting system for photocatalytic cross-coupling hydrogen evolution reaction, Angew. Chem. Int. Ed. 58 (2019) 8862–8866, doi:10.1002/anie.201904407.
- [81] Y. Cai, Y. Wang, C. Wang, R. Long, L. Cao, Y. Chen, Y. Yao, Hierarchical self-assembly of 3D amphiphilic discrete organoplatinum(II) metallacage in water, Chin. Chem. Lett. 31 (2020) 689–692, doi:10.1016/j.cclet.2019.08.036.
- [82] Y. Wang, C. Wang, R. Long, Y. Cao, D. Fan, M. Cen, L. Cao, Y. Chen, Y. Yao, Synthesis and controllable self-assembly of 3D amphiphilic organoplatinum(ii) metallacages in water, Chem. Commun. 55 (2019) 5167–5170, doi:10.1039/ C9CC02173F.
- [83] S. Saha, B. Holzapfel, Y.-.T. Chen, K. Terlinden, P. Lill, C. Gatsogiannis, H. Rehage, G.H. Clever, Rational design of an amphiphilic coordination cage-based emulsifier, J. Am. Chem. Soc. 140 (2018) 17384–17388, doi:10.1021/jacs. 8b10991.
- [84] W.M. Bloch, J.J. Holstein, B. Dittrich, W. Hiller, G.H. Clever, Hierarchical assembly of an interlocked M<sub>8</sub>L<sub>16</sub> container, Angew. Chem. Int. Ed. 57 (2018) 5534–5538, doi:10.1002/anie.201800490.
- [85] C.J. Pedersen, Cyclic polyethers and their complexes with metal salts, J. Am. Chem. Soc. (1967) 7017–7036.
- [86] C. Lu, M. Zhang, D. Tang, X. Yan, Z. Zhang, Z. Zhou, B. Song, H. Wang, X. Li, S. Yin, H. Sepehrpour, P.J. Stang, Fluorescent metallacage-core supramolecular polymer gel formed by orthogonal metal coordination and host-guest interactions, J. Am. Chem. Soc. 140 (2018) 7674–7680, doi:10.1021/jacs.8b03781.
- [87] D. Liu, H. Liu, B. Song, M. Chen, J. Huang, J. Wang, X. Yang, W. Sun, X. Li, P. Wang, Terpyridine-based metallo-organic cages and supramolecular gelation by coordination-driven self-assembly and host-guest interaction, Dalt. Trans. 47 (2018) 14227–14232, doi:10.1039/C8DT01044G.
- [88] Y. Wang, G. Ping, C. Li, Efficient complexation between pillar[5]arenes and neutral guests: from host-guest chemistry to functional materials, Chem. Commun. 52 (2016) 9858–9872, doi:10.1039/C6CC03999E.
- [89] Y. Liu, B. Shi, H. Wang, L. Shangguan, Z. Li, M. Zhang, F. Huang, Construction

- of metallacage-cored supramolecular gel by hierarchical self-assembly of metal coordination and pillar[5]arene-based host—guest recognition, Macromol. Rapid Commun. 39 (2018) 1800655, doi:10.1002/marc.201800655.
- [90] Y. Sun, F. Zhang, S. Jiang, Z. Wang, R. Ni, H. Wang, W. Zhou, X. Li, P.J. Stang, Assembly of metallacages into soft suprastructures with dimensions of up to micrometers and the formation of composite materials, J. Am. Chem. Soc. 140 (2018) 17297–17307, doi:10.1021/jacs.8b11199.
- [91] Y. Sun, Y. Yao, H. Wang, W. Fu, C. Chen, M.L. Saha, M. Zhang, S. Datta, Z. Zhou, H. Yu, X. Li, P.J. Stang, Self-assembly of metallacages into multidimensional suprastructures with tunable emissions, J. Am. Chem. Soc. 140 (2018) 12819– 12828, doi:10.1021/jacs.8b05809.
- [92] Y. Shi, M. Wang, C. Ma, Y. Wang, X. Li, G. Yu, A conductive self-healing hybrid gel enabled by metal-ligand supramolecule and nanostructured conductive polymer, Nano Lett. 15 (2015) 6276–6281, doi:10.1021/acs.nanolett.5b03069.
- [93] L. Zeng, Y. Xiao, J. Jiang, H. Fang, Z. Ke, L. Chen, J. Zhang, Hierarchical gelation of a  $Pd_{12}L_{24}$  metal–organic cage regulated by cholesteryl groups, Inorg. Chem. 58 (2019) 10019–10027, doi:10.1021/acs.inorgchem.9b01171.
- [94] P. Sutar, V.M. Suresh, K. Jayaramulu, A. Hazra, T.K. Maji, Binder driven self-assembly of metal-organic cubes towards functional hydrogels, Nat. Commun. 9 (2018) 3587, doi:10.1038/s41467-018-05818-w.